JGR Earth Surface

RESEARCH ARTICLE
10.1029/2019JF005004

A Numerical Model for Fluvial Transport of Subglacial Sediment

Ian Delaney[1,2], **Mauro A. Werder**[1], **and Daniel Farinotti**[1,3]

[1]Laboratory of Hydraulics, Hydrology and Glaciology (VAW), ETH-Zürich, Zürich, Switzerland, [2]Now at Jet Propulsion Laboratory, California Institute of Technology Pasadena, Pasadena, CA, USA, [3]Swiss Federal Institute for Forest, Snow and Landscape Research (WSL), Birmensdorf, Switzerland

Key Points:
- A numerical model for subglacial sediment transport is presented
- Constraining subglacial till connectivity and bedrock erosion is imperative to describing subglacial sediment discharge
- Model outputs can capture measured variations in subglacial sediment discharge with reasonable skill

Correspondence to:
I. Delaney,
delaney@vaw.baug.ethz.ch

Citation:
Delaney, I., Werder, M. A., & Farinotti, D. (2019). A numerical model for fluvial transport of subglacial sediment. *Journal of Geophysical Research: Earth Surface*, *124*, 2197–2223. https://doi.org/10.1029/2019JF005004

Received 9 JAN 2019
Accepted 10 JUL 2019
Accepted article online 21 JUL 2019
Published online 20 AUG 2019

Abstract Sediment discharge from glaciers impacts downstream aquatic habitats, hydropower operations, and river infrastructure. Since discharge of subglacial sediment will evolve in response to glacier retreat, estimating future subglacial sediment dynamics is of great relevance. To develop tools and methods to better constrain the responsible processes, we present a till dynamics model that accounts for limited sediment access coupled to a subglacial hydrology model to describe the evolution of a subglacial till layer over a glacier's longitudinal profile in one dimension. Synthetic simulations examining the effects of changing hydrology highlight the importance of properly constraining both the erosion of underlying bedrock and the subglacial sediment connectivity. This is because changes in hydrology alter the timing of peak sediment discharge but only marginally affect total sediment discharge once the subglacial sediment reservoir is exhausted. Model simulations for real-world glaciers yield insights into the distribution of sediment along the glacier bed, including locations where sediments are deposited or exhausted. Comparison between model results and field data shows that total and peak sediment discharge, as well as interannual variability, can be captured with acceptable skill for periods ranging from hours to decades. The results from this model show that modeling subglacial sediment transport on decadal to subdaily scales is possible but requires processes such as bedrock erosion and sediment connectivity to be considered.

1. Introduction

Glacierized regions expel massive amounts of sediment (e.g., Hallet et al., 1996), and increasing amounts of sediment could be discharged as glaciers retreat and their melt accelerates (e.g., Costa et al., 2018; Bendixen et al., 2017; Koppes & Montgomery, 2009; Koppes et al., 2009). These sediments can affect hydropower operations through turbine abrasion and reservoir infill (e.g., Anselmetti et al., 2007; Ehrbar et al., 2018; Thapa et al., 2005), as well as downstream ecosystems (e.g., Brown et al., 2007; Sigler et al., 2002) and infrastructure (e.g., Lancaster et al., 2012). Glacial sediments originate from either the subglacial or the periglacial environment (Delaney, Bauder, Huss, et al., 2018; Guillon et al., 2015). Periglacial environments often comprise loose, unconsolidated material exposed by glacier retreat (e.g., Church & Ryder, 1972; Warburton, 1990), but these environments can stabilize relatively quickly (Ballantyne, 2002; Lane et al., 2017). Larger amounts of sediment, instead, typically originate subglacially, especially in highly glacierized catchments (e.g., Guillon et al., 2015; Delaney, Bauder, Huss, et al., 2018).

In the subglacial environment, however, sediment is produced when glaciers erode their substrate (e.g., Hallet, 1981; Herman et al., 2015) through plucking or quarrying and abrasion of the bedrock by debris-laden ice (Alley et al., 1997; Iverson, 2012; Penck, 1905; Röthlisberger & Iken, 1981). The majority of this subglacial sediment is transported by fluvial activity in the subglacial drainage system (e.g., Collins, 1990; Richards & Moore, 2003; Walder & Fowler, 1994), although sediment deformation below the ice and entrainment of material into the ice can also contribute (Iverson & Semmens, 1995; Swift et al., 2018).

Subglacial sediment mobilization is dependent on both the amount of sediment available for transport by meltwater (e.g., Collins, 1996; Burke et al., 2015; Willis et al., 1996) and on the velocity of subglacial water flowing beneath the glacier (e.g., Ng, 2000; Walder & Fowler, 1994). The velocity of subglacial water is a function of the size of the subglacial conduits that the water flows through, the discharge of the water, and the gradient of the hydraulic potential. This is manifested in the Darcy-Weisbach relation for water flow

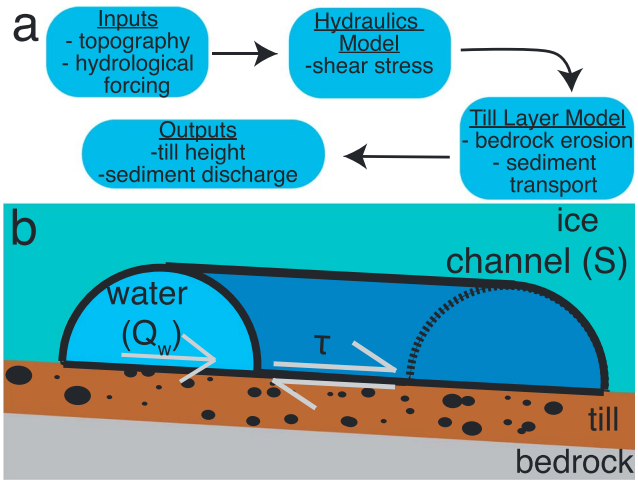

Figure 1. Model components (a) and cartoon of subglacial channel (b).

through a pipe (Beaud et al., 2018; Carter et al., 2017; Creyts et al., 2013; Hewitt & Creyts, 2019; Ng, 2000; Walder & Fowler, 1994). In a warming climate, glacier melt and water discharge will temporarily increase (e.g., Huss & Hock, 2018), resulting in a greater capacity of subglacial water to transport sediment. Furthermore, retreating mountain glaciers often steepen (e.g., Huss et al., 2010; Zekollari & Huybrechts, 2015), thus increasing both the hydraulic gradient (e.g., Flowers & Clarke, 1999) and the subglacial water velocity independently of the water discharge quantity. To determine how subglacial sediment dynamics will evolve in response to glacier retreat and hydrological changes, models are needed which account for (1) glacial erosion of bedrock (e.g., Koppes et al., 2009), (2) sediment supply (e.g., Bracken et al., 2015; Collins, 1996), (3) subglacial hydraulic gradients (e.g., Beaud et al., 2018; Flowers & Clarke, 1999), and (4) water discharge (e.g., Farinotti et al., 2012; Huss & Hock, 2018).

Here, we present a numerical model that captures sediment discharge based on the relationships between subglacial water flow, the hydraulic gradient at the glacier bed, the production of till, and the availability of subglacial sediment for transport by meltwater in one dimension along the glacier's longitudinal profile. A series of idealized test cases are used to assess the model's behavior and the potential changes in subglacial sediment yield associated with glacier retreat. The model is then calibrated, and its outputs are compared to suspended sediment discharge data collected from two glaciers and the total sediment discharge data collected from a third glacier in the Swiss Alps. By presenting the model and applying it to both idealized and real-world test cases, we introduce a numerical framework capable of predicting sediment discharge from glaciers in a changing climate.

2. Model Description

The model consists of two components which can describe subglacial sediment transport when coupled: (1) a water flow model, which captures the evolution of subglacial hydraulics in a channelized subglacial system, and (2) a till layer model, which provides a means to mobilize and deposit sediment, erode subglacial bedrock, and moderate the amount of sediment available for transport (Figure 1). Utilization of the model requires a description of glacier topography, which is collapsed to one dimension, and hydrological inputs.

In this work, we use the term *till* to describe the reservoir of sediment that lies beneath the glacier, while *sediment* is used to describe material that is mobilized, transported, or deposited in response to hydraulic conditions.

2.1. Hydraulics Model

Estimates of hydraulic conditions at the glacier bed over subdaily timescales are needed to describe the ability of subglacial water to transport sediment (e.g., Beaud et al., 2018; Collins, 1990; Creyts et al., 2013; Walder & Fowler, 1994). This is because water discharge often varies diurnally, while the subglacial drainage system responds over longer timescales (e.g., Iken & Bindschadler, 1986).

The model presented here is based upon the assumption that the water is transported through subglacial channels (Röthlisberger, 1972, Figure 1). Subglacial hydraulic conditions are constrained by using the assumption that, over sufficiently long timescales, the competing processes of ice deformation and channel wall melt are related to local water discharge. In particular, this allows us to define the size of the subglacial channels. As is common for glaciohydraulic models (e.g., Röthlisberger, 1972; Werder et al., 2013), we use the Darcy-Weisbach formulation for water flow through a pipe. Here, we relate the hydraulic diameter of the subglacial channel, D_h, to a representative water discharge, Q_w^*, and a representative gradient of hydraulic potential, Ψ^*

$$s f_r \rho_w \frac{Q_w^{*2}}{D_h^5} = \Psi^* . \quad (1)$$

Note that the hydraulic diameter, D_h, is defined as 4 times the ratio between the channel's cross-sectional area and its wetted perimeter. In the equation, f_r is the Darcy-Weisbach friction factor, ρ_w is the density

Table 1
Model Parameters That Remained Fixed Across All Model Runs With Their Value and Units

Name	Symbol	Value	Units
Darcy-Weisbach friction factor	f_r	0.15	—
Hooke angle of channel	β	30°	°
Darcy-Weisbach formula factor	s	0.12	—
Minimum hydraulic diameter[a]	$D_{\mathrm{h\,min}}$	0.21	m
Source quantile	s_{q}	0.75	—
Sediment-uptake *e*-folding length	l	100	m
Till height limit	H_{lim}	1.0	m
Till height erosion limit	H_g	0.75	m
Sediment connectivity factor	$\Delta\sigma$	1,000	m^{-1}
Gravitational constant	g	−9.81	$\mathrm{m/s}^2$
Density of water	ρ_{w}	1,000	$\mathrm{kg/m}^3$
Density of ice	ρ_{i}	900	$\mathrm{kg/m}^3$
Density of bedrock	ρ_{b}	2,650	$\mathrm{kg/m}^3$
Bulk density of sediment	ρ_{s}	1,500	$\mathrm{kg/m}^3$
Till porosity	ϵ	0	—
Glen's n	n	3	—
Ice flow rate factor	A	2.4×10^{-24}	$\mathrm{s/Pa}^3$
Valley shape factor	f_{s}	0.8	—
Mass-balance gradient	γ	0.00625	a^{-1}

[a]Corresponds to a minimal cross-sectional area of 0.25 m^2.

of water (Table 1), and s is a factor accounting for channel geometry (Hooke et al., 1990). The latter is calculated as

$$s = \frac{2(\beta - \sin\beta)^2}{(\frac{\beta}{2} + \sin\frac{\beta}{2})^4}\,, \tag{2}$$

where β is the central angle of the circular segment that comprises the channel (the so-called Hooke angle). Smaller values of β result in lower, broader channels, which may represent a less efficient drainage system, and $\beta = \pi$ corresponds to a semicircle, representing more efficient transport of meltwater. The width of the channel floor w_{c} is given by

$$w_{\mathrm{c}} = 2\sin\frac{\beta}{2}\sqrt{\frac{2S}{\beta - \sin\beta}}\,, \tag{3}$$

where S is the cross-sectional area of the channel given

$$S = \frac{D_{\mathrm{h}}^2}{2}\quad\frac{(\frac{\beta}{2} + \sin\frac{\beta}{2})^2}{\beta - \sin\beta}\,. \tag{4}$$

Melt opening and creep closure, which are characteristic of R-channels (Röthlisberger, 1972), are implicitly accounted for by choosing representative values of both discharge (Q_{w}^*) and gradient of the hydraulic potential (Ψ^*). Q_{w}^* is variable in both time and space, and its value for a horizontal location x along the glacier at time t is approximated by determining the quantile s_{q} of the instantaneous discharge Q_{w} at location x over the time interval $[t - \Delta t, t]$

$$Q_{\mathrm{w}}^*(x,t) = \mathrm{q}\left(Q_{\mathrm{w}}(x)\big|_{t-\Delta t}^{t}, s_{\mathrm{q}}\right)\,, \tag{5}$$

where q(…) is the function determining the quantile s_{q} of $Q_{\mathrm{w}}(x)$ for which s_{q} percent of water discharge over time period Δt is below that value. The instantaneous water discharge Q_{w} at a position x, $Q_{\mathrm{w}}(x)$ (Figure 2) is given by

$$Q_{\mathrm{w}}(x) = \int_{x_{\mathrm{top}}}^{x} m w \,\mathrm{d}x\,, \tag{6}$$

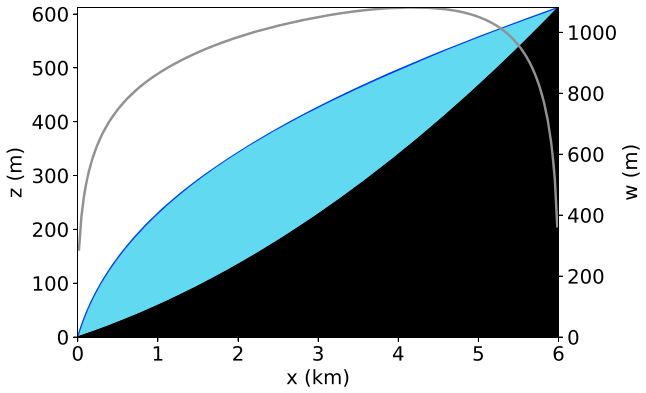

Figure 2. Idealized synthetic glacier geometry used in the test cases described in section 3. The geometry is based upon Bench Glacier (de Fleurian et al., 2018). The glacier's ice and bedrock are shown in blue and black, respectively. The gray line shows the glacier width w. Horizontal variable x and elevational variable z used in the model are labeled.

where m is the melt input per unit area, w is the glacier width (Figure 2), and x_{top} is the position of the top of the glacier.

We approximate the representative gradient of the hydraulic potential Ψ^* with the Shreve potential gradient

$$\Psi^* = \frac{\partial}{\partial x}(\rho_i g(z_s - z_b) + \rho_w g z_b)\,, \tag{7}$$

where z_s and z_b are the elevation of the glacier surface and bed, respectively, and ρ_i is the density of ice (Table 1). By inserting both Q_w^* and Ψ^* in equation (1), the hydraulic diameter D_h of the channel can be determined. For reasons discussed in section 2.4, a minimum hydraulic diameter $D_{h\,min}$ is prescribed, below which D_h cannot shrink.

Using the now-known D_h together with the instantaneous water discharge Q_w, equation (1) can be solved for the

$$\Psi = s f_r \rho_w \frac{Q_w^2}{D_h^5}\,. \tag{8}$$

This allows us to capture the short-term variations in the hydraulic gradient that are of relevance for sediment transport, which is often driven by relatively short term peaks in water flow.

2.2. Sediment and Till Dynamics Model

The quantity of sediment discharged from a glacier is determined using the Exner equation (Exner, 1920a, 1920b; Paola & Voller, 2005), a mass conservation equation which is applied to evolve the subglacial till layer of height H that lies across the width of the glacier bed

$$\frac{\partial H}{\partial t} w = -\frac{\partial Q_s}{\partial x}\frac{1}{1-\epsilon} + m_t w\,. \tag{9}$$

In this equation, Q_s is the sediment discharge, ϵ is the till porosity (Table 1), and m_t is a till source term which quantifies bedrock erosion rate per unit area.

In the model, the till mobilization $\frac{\partial Q_s}{\partial x}$ is determined by distinguishing three conditions

$$\frac{\partial Q_s}{\partial x} = \begin{cases} \dfrac{Q_{sc} - Q_s}{l} & \text{if } \dfrac{Q_{sc} - Q_s}{l} \le m_t w & \text{(10a)} \\ 0 & \text{if } H = H_{lim} \quad \& \quad \dfrac{Q_{sc} - Q_s}{l} \le 0 & \text{(10b)} \\ \dfrac{Q_{sc} - Q_s}{l}\sigma(H) + m_t w \cdot (1 - \sigma(H)) & \text{otherwise} & \text{(10c)} \end{cases}$$

where Q_{sc} is the sediment transport capacity (see equation (12) below), l is a sediment uptake e-folding length required for sediment discharge to adjust to transport capacity (e.g., Phillips & Sutherland, 1989), and H_{lim} is a maximum till thickness (Table 2) prescribed to prevent unbounded till deposition in places such as overdeepenings (e.g., Alley et al., 2003; Creyts et al., 2013; Werder, 2016). σ is a sigmoidal function of till height H

$$\sigma(H) = \left(1 + \exp\left(\frac{2 - \Delta\sigma H}{5}\right)\right)^{-1}, \tag{11}$$

and it is used for a smooth transition over $H = 2\Delta\sigma^{-1} \pm \Delta\sigma^{-1}$ in equation 10c. In the following, the value $\Delta\sigma$ is referred to as the sediment connectivity factor that describes the access of meltwater in the channel to sediment persisting laterally across the glacier bed (Table 1).

The three cases of equation 10 can be interpreted as follows: (1) Equation 10c encodes both the transport- and supply-limited case, with a smooth transition between the two (Figure 3), and allows some till to persist at the glacier bed when H is small. When $H \gg 2\Delta\sigma^{-1}$, the first term dominates and the system is in a transport-limited regime. In this case, till mobilization is such that sediment transport Q_s adjusts to capacity Q_{sc} with sediment uptake e-folding length l. When $H \ll 2\Delta\sigma^{-1}$, the second term dominates, and the

Table 2
Variables Used in the Model With Units

Name	Symbol	Units
Horizontal, vertical, and time coordinates	x, z, t	m, m, s
Glacier width, surface, and bed elevation	w, z_s, z_b	m, m, m
Glacier surface slope	α	—
Channel hydraulic diameter	D_h	m
Width of channel floor	w_c	m
Channel cross-sectional area	S	m^2
Water discharge (instantaneous)	Q_w	m^3/s
Water discharge at terminus (instantaneous)	Q_w^0	m^3/s
Representative water discharge	Q_w^*	m^3/s
Hydraulic potential	ϕ	Pa
Gradient of ϕ	Ψ	Pa/m
Representative gradient of ϕ	Ψ^*	Pa/m
Water velocity	v	m/s
Water shear stress	τ	Pa
Till source term	m_t	m/s
Sediment discharge	Q_s	m^3/s
Sediment discharge at terminus	Q_s^0	m^3/s
Sediment discharge capacity	Q_{sc}	m^3/s
Sediment concentration	C_s	kg/m^3
Sediment concentration at terminus	C_s^0	kg/m^3
Sediment concentration capacity	C_{sc}	kg/m^3
Sediment concentration capacity at terminus	C_{sc}^0	kg/m^3
Glacier sliding velocity	u_{sl}	m/s
Erosion rate	$\dot{e}$	m/s
Till layer height	H	m
Mass-balance rate at terminus	$\dot{b}^0$	m/s
Water source term	m	m/s

system is in a supply-limited regime where the supply is set as the glacier's width-integrated erosion rate $m_t w$. The transition between the two cases is smoothed over a span of $H \approx 2\Delta\sigma^{-1} \pm \Delta\sigma^{-1}$. This can be interpreted as a simple sediment connectivity model: as H drops below $3\Delta\sigma^{-1}$, access to till becomes limited and its mobilization decreases. Yet some sediment remains, which enables some transport during events when transport capacity is high (Wolman & Miller, 1960). Values for $\Delta\sigma$ are discussed in sections 2.4 and 5.2. (2) Equation 10a states that the system is in a transport-limited regime when the transport capacity is below the width-integrated erosion rate. (3) Equation (10b), finally, prevents unrealistic amounts of till from accumulating by imposing a maximum till thickness H_{lim}. If H reaches this limit, deposition ceases and more sediment is thus transported down glacier than transport conditions would allow, that is, $Q_s > Q_{sc}$.

The sediment transport capacity Q_{sc} is computed using the total load sediment transport formula by Engelund and Hansen (1967)

$$Q_{sc} = \frac{0.4}{f_r} \frac{1}{D_{m_{50}} (\frac{\rho_s}{\rho_w} - 1)^2 g^2} \left(\frac{\tau}{\rho_w} \right)^{\frac{5}{2}} w_c \,, \tag{12}$$

where ρ_s is the bulk density of the sediment (Table 1), $D_{m_{50}}$ is the mean sediment grain size (used as a calibration parameter; Table 3), and τ is the shear stress between the water and the channel bed. The latter is determined through the Darcy-Weisbach formulation

$$\tau = \frac{1}{8} f_r \rho_w v^2 \,, \tag{13}$$

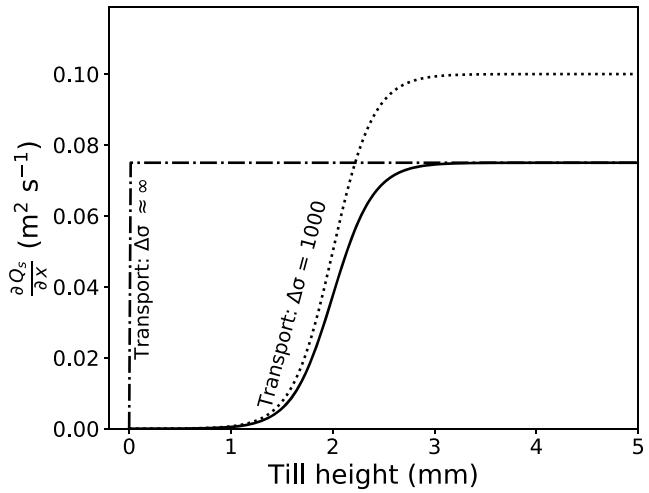

Figure 3. Sediment mobilization ($\frac{\partial Q_s}{\partial x}$) versus till height for two different sediment connectivity factors ($\Delta\sigma$) and for two different transport capacities (with m_t and Q_s set to 0). Dashed line: perfect sediment connectivity $\Delta\sigma \approx \infty\,\mathrm{m}^{-1}$. Solid line: connectivity $\Delta\sigma = 1,000\,\mathrm{m}^{-1}$. Dotted line: also $\Delta\sigma = 1,000\,\mathrm{m}^{-1}$ with increased transport capacity.

where $v = \frac{Q_w}{S}$ is the water velocity. Note that because shear stress τ is used to couple hydraulic conditions to sediment transport, alternative sediment transport relationships (e.g., Meyer-Peter & Müller, 1948) can be implemented. Actual (C_s) and transport capacity (C_{sc}) sediment concentrations can be calculated with

$$C_s = \frac{\rho_s Q_s}{Q_w} \quad \text{and} \quad C_{sc} = \frac{\rho_s Q_{sc}}{Q_w}\,, \tag{14}$$

respectively.

New till is created by eroding subglacial bedrock by processes such as quarrying and abrasion (e.g., Alley et al., 1997; Hallet, 1979; Herman et al., 2015). The till source term m_t (equation (9)) is assumed to be a linear function of both the base erosion rate $\dot{e}$ and the till layer thickness H

$$m_t = \begin{cases} \dot{e}(H_g - H) \\ 0 \end{cases} \quad \text{if } H \geq H_g\,. \tag{15}$$

In the above equation, H_g is a predefined till thickness beyond which no further erosion occurs (Table 2; Brinkerhoff et al., 2017). The erosion rate itself is assumed to be proportional to the glacier sliding speed u_{sl} and is calculated following the linear relationship presented in Herman et al. (2015)

$$\dot{e} = 10^{-4}\, u_{sl}\,. \tag{16}$$

u_{sl} is assumed to be a given fraction f_{sl} of the ice deformation velocity (e.g., Huss & Farinotti, 2014) and is calculated via the shallow ice approximation (Hutter, 1983)

$$u_{sl} = f_{sl}\,\frac{2A}{n+1}\,(f_s\,\rho_i\,g\sin\alpha)^n\,(z_s - z_b)^{n+1}. \tag{17}$$

Here, n is Glen's exponent, A is the ice flow rate factor, f_s is a valley shape factor (Table 1), and α is the surface slope.

2.3. Numerical Implementation

Equation (9) is discretized in space using a finite volume scheme. The resulting system of ordinary differential equations for till layer height H is time stepped using the VCABM solver (Hairer et al., 1993; Radhakrishnan & Hindmarsh, 1993) from the package *DifferentialEquations.jl* (Rackauckas & Nie, 2017). Experience with the model suggests that the spatial discretization should be substantially smaller than sediment uptake e-folding length l (equation 10), typically requiring a resolution of less than 60 m. To test the model performance with respect to solver tolerance and grid size, modeled till heights obtained over 1 year of idealized hydrological forcing were compared to a reference run with very small grid size (1 m) and solver tolerances of 10^{-10} m. Annual errors in till height were assumed to be the difference between these two runs and should be substantially lower than the typical erosion rates in glacierized catchments (~1 mm; Hallet et al., 1996). The analysis indicates that both absolute and relative solver tolerance (Rackauckas & Nie, 2017) should be below 10^{-6} m and that grid cells of less than approximately 30 m are advisable (Figure 4). A maximum time step of 6 hr was imposed to ensure that all diurnal variations were captured.

Using the tolerances and grid spacing suggested above, a year of model time takes from 5 to 30 s wall-time and is mainly dependent on factors such as variability in water input and glacier topography. Increased variability in glacier topography and water input, mainly in real glacier applications (section 4), leads to increased computational costs.

Table 3
Model Tuning Parameters

Name	Symbol	Units	Value for idealized test case
Smoothing period of Q_{sm}	Δt	s	1.5 days
Sliding fraction	f_{sl}	—	2.5
Mean sediment grain size	$D_{m_{50}}$	m	0.04 m

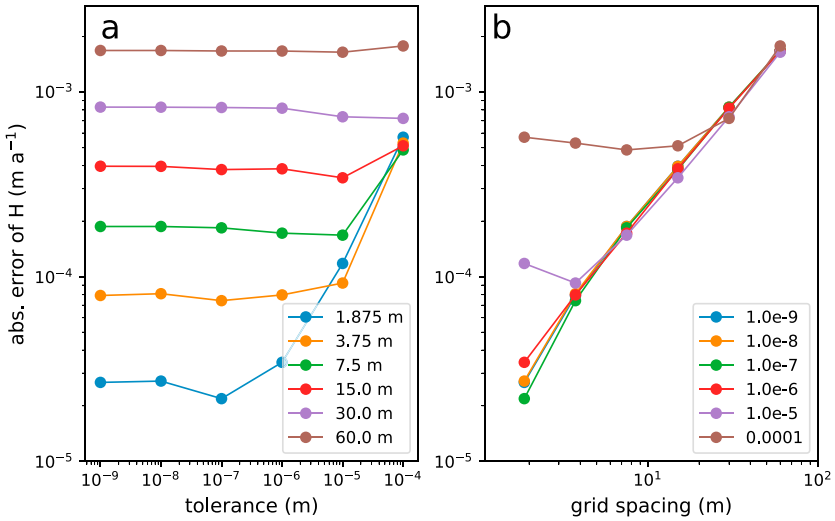

Figure 4. Error (i.e., difference to the reference model run) in till layer height (H) versus (a) solver tolerances (both absolute and relative; Rackauckas & Nie, 2017) and (b) grid spacing. Lines of a given color represent a suite of tests with consistent grid spacing (a) or tolerance (b).

2.4. Model Parameters and Fitting

The model contains 21 parameters (Table 1) of which half are not well constrained. The parameters are set within a range supported by the literature, or, in selected cases, manually tuned to plausible values. We acknowledge that this situation is far from ideal, but note that this is often encountered in subglacial process models (e.g., Werder et al., 2013) since the lack of data does not allow for more rigorous constraints on parameters.

The Darcy-Weisbach friction factor is set to $f_r = 0.15$, which is at the upper range of reported values (Clarke, 2003; Werder et al., 2010), although substantially higher values could be possible (Chen et al., 2018). The Hooke angle of $\beta = 30°$ is close to the 36° inferred for Gornergletscher (Hooke et al., 1990) and creates a low and broad channel shape. The source quantile s_q is set to 0.75. f_r, β, and s_q are set such that the instantaneous hydraulic potential ϕ does not reach exceedingly high values above the flotation hydraulic potential. The minimum hydraulic diameter, $D_{h\,min}$, is set to 0.2 m, which ensures that there are no unphysical spikes in both instantaneous gradients of hydraulic potential Ψ and sediment discharge at the onset of the melt season caused by large amounts of melt water flowing through a small channel. The ice flow parameters $n = 3$ and $A = 2.4\times10^{-24}$ s/Pa^3 are at their standard values for temperate ice (Cuffey & Paterson, 2010), with the valley shape factor $f_s = 0.8$ corresponding to a glacier four times wider than thick.

The bulk density of sediment is $\rho_s = 1,500$ kg/m^3, the same as assumed in Delaney, Bauder, Werder, et al., (2018), while till density is set to $\rho_b = 2,650$kg/m^3, which is the density of granite bedrock. To avoid density conversions, porosity ϵ is zero. The sediment uptake e-folding length l describes the distance along the subglacial channel for sediment to respond to sediment transport conditions. It depends on the grain size (Creyts et al., 2013) and is set to $l = 100$ m. The till height limit is set to $H_{lim} = 1$ m to allow some till to accumulate below the glacier but to keep the reservoir small, and thus the model avoids excessive deposition of sediment in overdeepenings (Alley et al., 2003). Although till heights of far over 1 m have been observed in subglacial environments (e.g., Truffer et al., 2001), this till height was chosen given the need for moderating feedback (discussed further in section 5.1). Higher values would likely only prolong the model response time and minimally affect the sediment discharge at the glacier snout once the till layer is in equilibrium. The sediment connectivity factor which controls the transition between supply and transport limited regimes is $\Delta\sigma = 1,000$ m^{-1}. This value was chosen such that seasonal sediment discharge is in line with measurements. The implications of this value are discussed in section 5.2.

Calibrating the model to sediment discharge from the glacier terminus means adjusting the spatial distribution of till along the glacier bed to a point measurement at the glacier terminus. Additionally, the large number of parameters mean that many parameter combinations could be found which lead to an acceptable fit. However, here, three model parameters (Table 3) are used to calibrate the model to sediment discharge

measurements. (1) The mean sediment grain size $D_{m_{50}}$ m, was chosen because it controls the amount of transported sediment via equation (12). (2) The glacier's sliding fraction $f_{sl}(-)$, which was selected because it influences till production and sediment availability (equations (17) and (15)). (3) Finally, the period Δt (s) over which water discharge Q_w is smoothed to obtain the representative water discharge value Q_w^* was chosen because it moderates the water velocity in the hydraulics model (equation (1)). It is necessary to find an adequate value for f_{sl} in calibrating the model because this term describes the supply of sediment, which must be above a certain quantity for the model to perform adequately. We acknowledge, however, that other parameter combinations, such as including source quantile s_q or friction factor f_r, could be used to calibrate the model and control the amount of sediment discharge.

Variables with a superscript 0 (encountered later in the text and figures) denote quantities at the glacier terminus. For instance, Q_w^0 and Q_s^0 represent proglacial discharge of water and sediment, respectively (Table 2).

3. Model Response in Idealized Test Cases

3.1. Test Case Description

Idealized test cases were used to assess the model's response to seasonal and diurnal variations in discharge. The test cases are based on a synthetic geometry which mimics Bench Glacier (Figure 2), introduced by the Subglacial Hydrology Model Intercomparison Project (SHMIP; de Fleurian et al., 2018).

Parameterization of glacier hydrology was also inspired by the temperature index model presented in SHMIP. Here the melt model calculates water input $m(x)$ (required by equation (6)) as a function of instantaneous temperature $T(z_s)$ at surface elevation $z_s(x)$

$$m(z_s) = \begin{cases} M_f\, T(z_s) & \text{if } T(z_s) > 0 \\ 0 & \text{if } \quad T(z_s) \le 0 \end{cases}, \tag{18}$$

where $M_f = 0.01\ \mathrm{m \cdot K^{-1} \cdot d^{-1}}$ is a melt factor and $T(z_s)$ is air temperature at elevation z_s. The latter is defined by

$$T(z_s) = \left(-A_a \cos\left(\frac{2\pi t}{s_{year}}\right) + A_d \cos\left(\frac{2\pi t}{s_{day}}\right) + \Delta T - 5 \right) \cdot \left(1 + z_s \frac{dT}{dz}\right), \tag{19}$$

where A_a and A_d are the annual and diurnal amplitudes, respectively, ΔT is a temperature offset which is adjusted control the meltwater input, s_{year} and s_{day} are the number of seconds in a year and in 1 day, respectively, and $dT/dz = -0.0075$ K/m is a temperature lapse rate. As the maximum time step of the solver (6 hr) resolves daily variations in melt, variability in the time steps themselves from the solver negligibly affect the melt rate. This is noted, as over longer time periods (days to months) different melt quantities are produced with constant melt factors (Hock, 2003). The experiments presented in the following section will examine the model response to variations in ΔT and A_d, while A_a is set to 16 °C.

3.2. Model Response to Temperature

Five temperature scenarios ($\Delta T = [-4, -2, 0, +2, +4]$°C, $A_d = 1$ °C; equation (19)) were investigated to assess how differences in meltwater input alter subglacial sediment discharge. No till ($H = 0$ m) was imposed at the beginning of the simulation. The model was run for a 15-yr period, which allowed an equilibrium to be reached between the annual amounts of bedrock erosion and sediment transport.

Model simulations over a 15-year period show that higher water input caused by higher temperature scenarios results in greater total sediment discharge (Table 5). In particular, higher temperatures induce increased meltwater amounts at the glacier's higher elevations, thus increasing the portion of the glacier bed where sediment transport can occur. The existence of such a positive correlation between seasonal water input and sediment discharge has been observed in some field-based experiments as well (e.g., Stott & Mount, 2007). In observational studies, this relationship could also be due to increased bedrock erosion following greater sliding (Koppes et al., 2015; Herman et al., 2015), a process not accounted for in this model.

Lower temperature scenarios result in slightly smaller sediment totals being evacuated, yet mean sediment concentrations are higher. The resulting concentrations are consistent with those found in field observations (e.g., Swift et al., 2005; Willis et al., 1996). These model results show that smaller water inputs are more efficient at transporting sediment than larger water quantities (Table 5). This is because the test cases occur

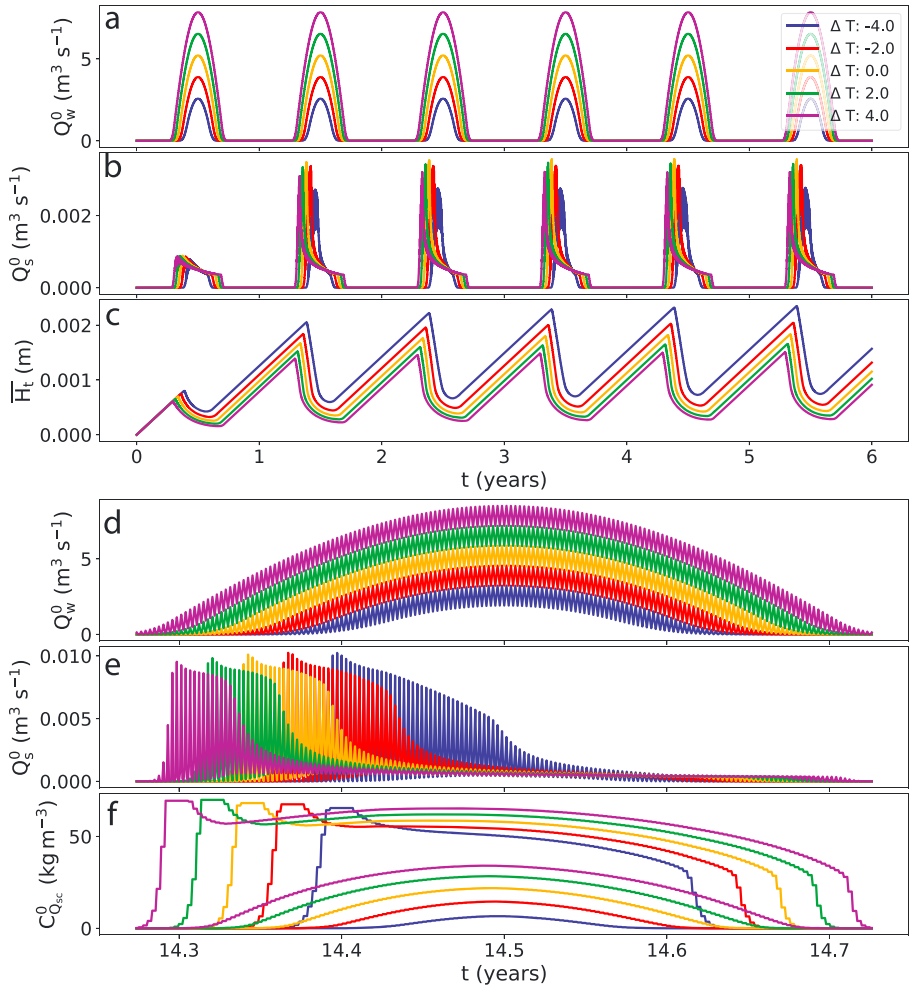

Figure 5. Select periods of a 15-year model run of a synthetic valley glacier (Figure 2) with variable temperature offsets ΔT (equation (19)) dictating total water input. (a, d) Water discharge at the terminus Q_w^0. (b, e) Sediment discharge at the terminus Q_s^0. (c) Average till layer height across the glacier bed $\bar{H}$. (f) Maximum and minimum daily sediment concentration capacity at terminus C_{sc}^0. Panels (a)–(c) show the first 6 years of the model run after which $\bar{H}$ reaches a steady annual cycle. Here, Q_s^0 and Q_w^0 are smoothed for clarity. Panels (d)–(f) show year 15 of the simulation, with Q_w^0 and Q_s^0 that are not smoothed.

in a sediment supply-limited regime, where increasing water discharge does not result in greater amounts of sediment transport. In response, sediment concentrations at the terminus, C_s^0, are a function of dilution of the sediment in the meltwater, not the mobilization of sediment.

The time period required to reach a steady annual cycle depends on the meltwater input (Figure 5). Over simulated annual time periods, glacier erosion at the beginning of the run exceeds the total amount of sediment transport. This causes the subglacial till layer height to grow for a certain period, before an equilibrium is reached. This occurs mainly on the upper reaches of the glacier, where sediment transport capacity is minimal. Later, glacier erosion decreases in regions of the bed where meltwater does not transport away all till, because of the increased thickness of the till (equation (15)). An equilibrium is reached between till production and transport in this case. The equilibrium is reached more quickly in high temperature scenarios compared to low temperature ones.

On the seasonal scale, peak sediment discharges are slightly higher in lower temperature scenarios (Figure 5e). This results from increased amounts of sediment that accumulate during the winter months, and from the fact that melt initiates later in the year for the low temperature cases. The latter allows additional till to build up. Conversely, sediment concentration capacity at the terminus, C_{sc}^0, varies only minimally with the differing scenarios and occurs early at the onset of melt. As a result, changes to glacier melt can cause

Table 4
Hydrological Forcing Parameters for Experiments Examining Synthetic Test Cases

Test	Seasonal offset ΔT °C	Seasonal variability A_a °C	Diurnal variation A_d °C
Increasing seasonal input	[−4, −2, 0, 2, 4]	16	1
Diurnal variability	0	16	[2 1 0.5 0.25 0.1]

some changes to sediment transport capacity, but the predominant differences result from the availability of till for transport. In turn, once available till is exhausted, typically in the last quarter of the season, sediment discharge is approximately equal to the rate of glacier erosion, with some diurnal variations until melt ceases (Figures 5d–5f). Sediment concentration capacity (Figure 5f) is on the order of the observed peak events (e.g., Felix et al., 2016) when till availability is likely ample. This shows the ability of this test case to capture observed quantities of discharge and concentreation.

The model results support the observation that till is quickly evacuated after its creation when sufficient melt is present (Herman et al., 2015; Riihimaki et al., 2005) and, thus, that a high sediment connectivity persists (e.g., Bracken et al., 2015; Mao et al., 2014). Additionally, it is observed that coincident variations in sediment and water discharge are limited to periods during which till storage is not exhausted (Delaney, Bauder, Werder, et al., 2018).

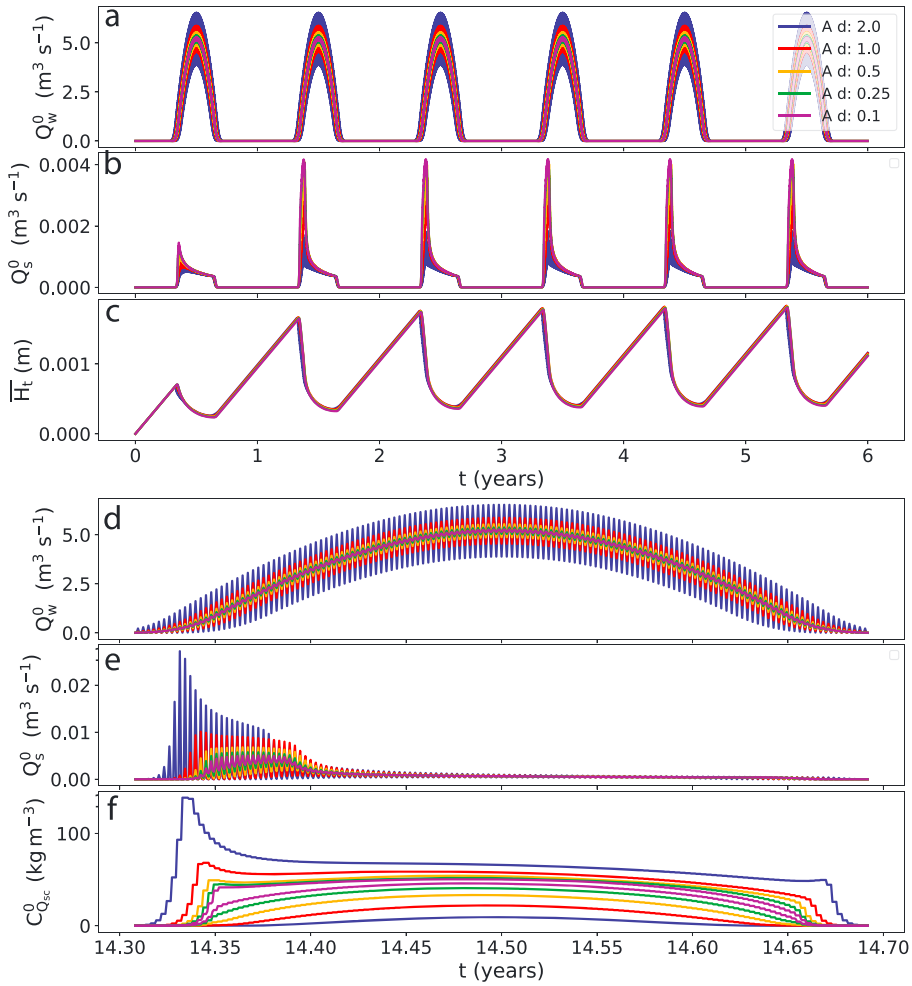

Figure 6. Same as Figure 5 but for changing diurnal amplitude A_d (equation (19)).

Table 5
Sediment Discharge, Water Discharge, and Mean Sediment Concentration for Synthetic Test Cases

	15-year run			Annual cycle		
Test	$\sum Q_s^0$ (m^3)	$\sum Q_w^0$ (m^3)	$\overline{C_s}$ (kg/m^3)	$\sum Q_s^0$ (m^3)	$\sum Q_w^0$ (m^3)	$\overline{C_s}$ (kg/m^3)
			Temperature			
ΔT: −4 °C	162,300	1.90×10^8	1.28	11,400	1.27×10^7	1.34
ΔT: −2 °C	163,900	3.48×10^8	0.71	11,400	2.32×10^7	0.74
ΔT: 0 °C	165,000	5.40×10^8	0.47	11,400	3.60×10^7	0.48
ΔT: 2 °C	165,800	7.60×10^8	0.33	11,500	5.06×10^7	0.34
ΔT: 4 °C	166,500	10.1×10^8	0.25	11,500	6.70×10^7	0.26
			Diurnal variability			
A_d: 2 °C	165,000	5.45×10^8	0.45	11,500	3.60×10^7	0.48
A_d: 1 °C	165,000	5.40×10^8	0.46	11,400	3.60×10^7	0.48
A_d: 0.5 °C	165,100	5.38×10^8	0.46	11,400	3.60×10^7	0.48
A_d: 0.25 °C	165,200	5.38×10^8	0.45	11,400	3.60×10^7	0.48
A_d: 0.1 °C	165,300	5.38×10^8	0.45	11,400	3.60×10^7	0.48

Note. The "15-year" quantities on the left represent metrics over the entire model run, where as the "annual cycle" on the right refers to yearly metrics once a steady annual cycle has been reached.

3.3. Model Response to Diurnal Variations in Temperature Amplitude

The response of subglacial sediment discharge to changes in the amplitude of diurnal water discharge has been documented (e.g., Swift et al., 2005; Willis et al., 1996). In this suite of experiments, the diurnal amplitude (A_d) is varied by 0.1, 0.25, 0.5, 1, and 2 °C (Table 4 and equation (19)), similar to the seasonal forcing applied to Suite C in SHMIP (de Fleurian et al., 2018). The temperature offset in the melt model remains constant ($\Delta T = 0$ °C). Nevertheless, higher amplitude scenarios result in slightly greater total water discharges as higher peak temperatures cause additional melt.

Similar to the scenarios presented in section 3.2, a steady annual cycle is reached after only a couple of years, once an equilibrium between glacier erosion and sediment transport is established (Figure 6 and Table 5). Higher peak sediment discharges occur in higher variability runs, due to higher water discharges, which allows for access to additional till by melt water compared to other runs. Additionally, high-amplitude runs also cause a greater disparity between the representative discharge Q_w^* (equation (5)) and the instantaneous discharge Q_w. This results in higher water velocities, which in turn allow greater amounts of sediments to be transported (sections 2.1 and 2.2).

The total amounts of discharged sediment are similar for all cases (Table 5). This experiment examining diurnal variations in glacier melt shows that sediment mobilized in the model's subglacial environment is greatly influenced by bedrock erosion (e.g., Herman et al., 2015) and not only by hydrological drivers. Glacier erosion alone, however, is a poor proxy for sediment discharge on subseasonal and decadal scales, as no mechanism exists for the material to be transported from the glacier bed to its terminus. In such cases, changes in hydrology become important, as they can alter the portion of the bed where transport can take place (e.g., Collins, 1996).

3.4. Examination of Diurnal Model Behavior and Hysteresis

The relationship between sediment and water in the subglacial system has been used to interpret glaciological processes (e.g., Perolo et al., 2018) and has given insight into the availability of sediment beneath glaciers (e.g., Riihimaki et al., 2005; Swift et al., 2005; Willis et al., 1996). Therefore, describing the capacity of a model to capture these processes is useful in presenting its ability to capture real-world phenomena (Beaud et al., 2018). Here, the model is run with the parameters presented in Table 4 for a melt season (Figure 4).

The model shows a relatively strong clockwise hysteresis early in the melt season (black stars and crosses, Figure 7), which show depletion of subglacial sediment over the day as has been documented in many field observations (e.g., Riihimaki et al., 2005; Singh et al., 2005). In the middle of the season, with the highest water discharges (gray stars and crosses, Figure 7), the clockwise hysteresis is present but less pronounced.

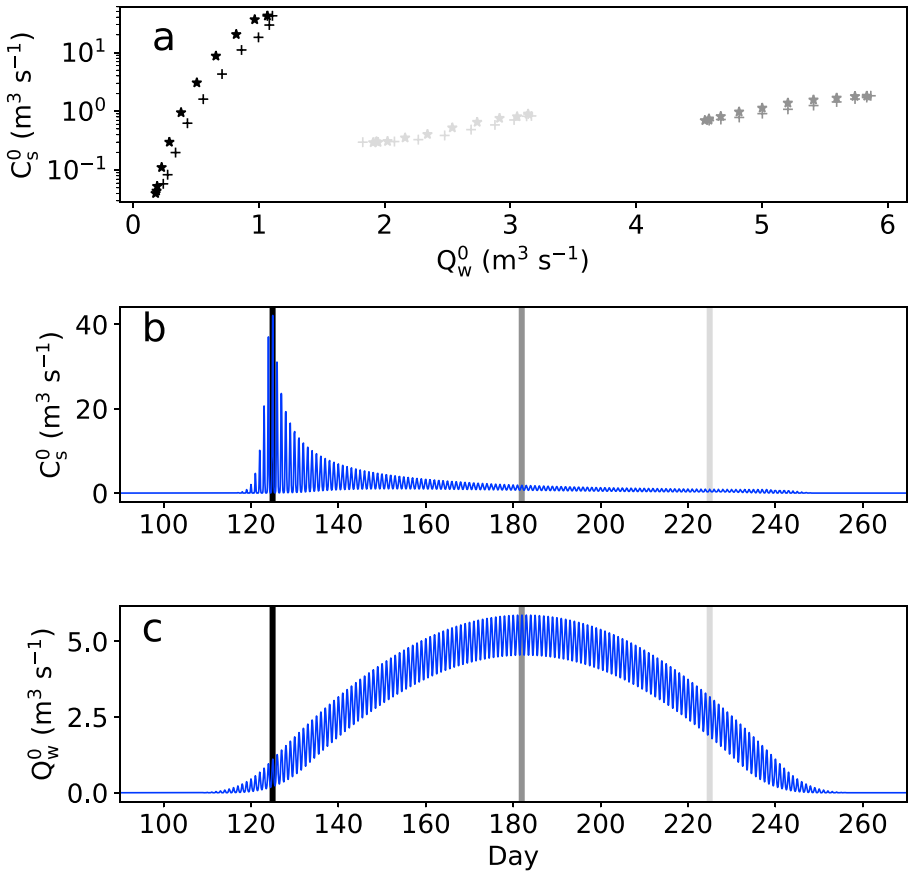

Figure 7. Hysteresis (a) between sediment concentration (b) and water discharge (c) through the melt season. Stars represent the rising limb of the hydrograph, while plus signs represent the falling limb. Note the slight clockwise hysteresis.

Finally, at the end of the melt season (light gray stars and crosses, Figure 7), only minimal hysteresis can be identified. This suggests the diurnal variability in sediment access decreases beyond the initial peak in suspended sediment concentration early in the season (Williams, 1989). However, counterclockwise hysteresis is not observed in these model outputs as is sometimes observed in natural systems (e.g., Mao et al., 2014; Riihimaki et al., 2005) and in model outputs (Beaud et al., 2018). In the modeling framework presented here, this could be due to the relatively steep hydraulic gradients of the synthetic glacier (Figure 2) that do not permit deposition of substantial amounts of sediment at the terminus that could permit counterclockwise hysteresis in these environments.

4. Comparison With Real-World Observations

4.1. Study Sites and Model Setup

The model performance is assessed for three sites in the Swiss Alps including the catchments of Gornergletscher, Aletschgletscher, and Griesgletscher. The sites are selected because of the availability of (1) measured subglacial sediment discharge in catchments where subglacial erosion can be isolated (Bezinge, 1987; Collins, 1979, 1989, 1996; Delaney, Bauder, Huss, et al., 2018; Delaney, Bauder, Werder, et al., 2018), (2) measured or reconstructed catchment runoff (Delaney, Bauder, Huss, et al., 2018; Delaney, Bauder, Werder, et al., 2018), and (3) measured and reconstructed subglacial topography (Farinotti et al., 2009; Huss & Farinotti, 2012).

The availability of this sediment discharge data provides the opportunity to calibrate the model and assess its performance. Annual totals of sediment discharge can be used to examine the model's ability to capture both longer-term variations and interannual variability. Seasonal data can also be used to examine the model's ability to capture short-term variations in sediment discharge.

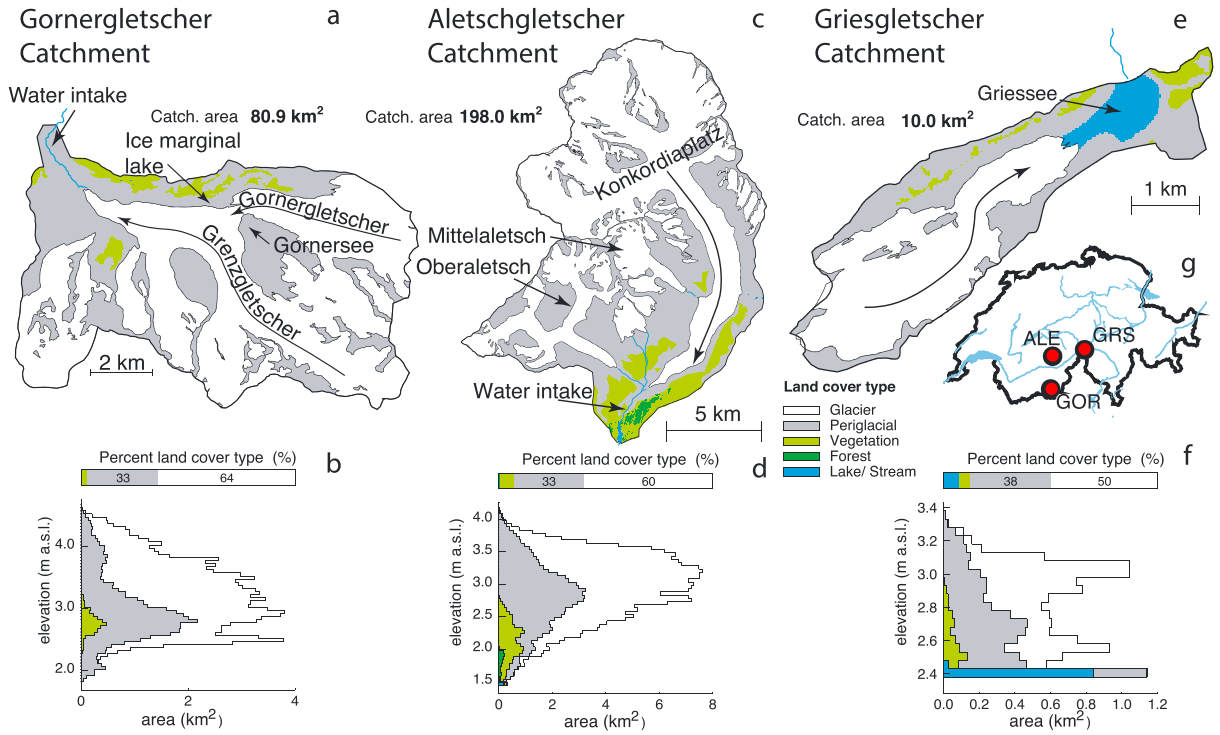

Figure 8. Overview of the investigated real-world catchments. Maps of the catchments (a, c, e) are given together with the corresponding hypsometry and land cover (b, d, f). The location within Switzerland is shown in panel (g). Land cover types are noted. Approximate flow lines are shown with arrows. Water intakes which house instrumentation are marked for the Gornergletscher (a) and Aletschgletscher (c) catchments.

4.1.1. Gornergletscher

Gornergletscher (Figure 8a) lies within a catchment of 75 km^2 and consists of two large tributaries, Gornergletscher and Grenzgletscher, and several smaller ones. Over the past decades, the glacier has been the subject of considerable research pertaining to subglacial hydrology and sediment dynamics (e.g., Bezinge, 1987; Collins, 1979; Werder et al., 2010). A large glacial lake, Gornersee, has historically formed at the confluence of the two tributaries, resulting in regular glacier lake outburst floods (e.g., Werder & Funk, 2009). In more recent years, an ice marginal lake forms slightly downstream. Its prolonged drainage is characterized by high sediment concentrations (Delaney, Bauder, Werder, et al., 2018). Additionally, an overdeepening is present at the glacier terminus (Figure 14a).

Water discharge data for the catchment are available at a water intake (location: 45°59′25”N, 7°43′50”E) used by the hydropower company, Grande Dixance. A turbidity meter and water sampler were installed approximatively 500 m from the intake to collect data over the 2016 and 2017 seasons, while historical sediment discharge data are available from Collins (1989) and Collins (1990) and Bezinge (1987). A detailed description of the data set can be found in Delaney, Bauder, Werder, et al. (2018).

4.1.2. Aletschgletscher

The Aletschgletscher catchment (Figure 8b) is 190 km^2 in size and comprises the three subcatchments of the Grosser Aletschgletscher (135 km^2), the Mittelaletschgletscher (15 km^2), and the Oberaletschgletscher (40 km^2). Water discharge is available from a station of the Swiss Federal Office for the Environment (station location: 46°23′09”N, 8°00′25′E). Suspended sediment discharge has been measured roughly 200 m downstream of the water discharge station over the 2016 and 2017 field seasons (Figure 8b). A full description of the data set can be found in Delaney, Bauder, Werder, et al. (2018).

4.1.3. Griesgletscher

The Griesgletscher comprises roughly 50% of the 10-km^2 catchment (Figure 8c), which is bound by a dammed hydropower reservoir at its outlet. Modeled catchment runoff, constrained with observational data, is available at hourly resolution from Delaney, Bauder, Huss, et al. (2018). Subglacial sediment discharge was determined for the period from 2011 to 2016 at an annual resolution from repeat bathymetry of the proglacial reservoir. The relative contribution of proglacial sediment discharge was determined for the period from

Table 6
Description of Real-World Experiments

Glacier	Time period (spin-up period)	Skill metrics analyzed[a]	Adequate model run conditions	Best fit parameters		
				Δt (hr)	f_{sl} ()	$D_{m_{50}}$ (m)
High resolution						
Gornergletscher	2014–2017 (2011–2013)	NSE_{24hr}, ERR_{24hr}, $TERR$	$NSE_{24hr} \geq 0.5$	102	1.725	0.062
Aletschgletscher	2014–2017 (2011–2013)	NSE_{24hr}, ERR_{24hr}, $TERR$	$NSE_{24hr} \geq 0.5$	192	0.85	0.032
Prolonged						
Griesgletscher	2009–2016 (2007–2008)	$RANK$, ERR_{sp}, $TERR$	$RANK = 1$	53	0.36	0.15
Gornergletscher	1973–2017 (1969–1972)	$RANK$, ERR_{sp}, $TERR$	$RANK \geq 0.7$	10	0.50	0.105

[a]See equations (21), 22, and 23.

1986 to 2014 in Delaney, Bauder, Huss, et al. (2018) and subtracted from the total changes in reservoir volume in 2015 and 2016 to determine the amount of subglacial sediment discharge. Similar to Gornergletscher, a small overdeepening is present near the glacier terminus (Figure 14g).

4.1.4. Parameterization of Hydrology and Glacier Topography

As explained in section 2.1, model operation requires describing water discharge at the glacier bed. Here, it is assumed that water input at a location in the catchment, $m(x)$, can be described by a melt rate $\dot{b}^0$ at the glacier terminus (elevation z_s^0), a mass balance gradient γ, and local elevation $z_s(x)$

$$m(x) = \dot{b}^0 + \gamma(z_s(x) - z_s^0)\,. \tag{20}$$

Since the total water yield at the glacier terminus, Q_w^0, is known from measurements (see previous subsections) and since γ is estimated to be close to values determined in Huss et al. (2008), the above expression can be substituted into equation (6) and solved numerically for $\dot{b}^0$. This allows us to obtain $m(x)$, and thus $Q_w(x)$, at every time step.

Given the one-dimensional nature of the model, the measured glacier topography must be reduced to one dimension. This is done using the method of Huss and Farinotti (2012), where gridded glacier surface and bed elevation data are collapsed over a given elevation band. For bed elevations, minimum elevations within an elevation band are chosen, as it is assumed that the majority of the subglacial water flow will occur at the lowest elevations of the glacier bed (thalweg).

4.2. Model Fitting Procedure and Skill Metrics

To calibrate the model, grid searches were conducted over the parameter space created by the three tuning parameters Δt ([5 hr, 168 hr], 11 steps), f_{sl} ([0.5, 2.25], 11 steps) and $D_{m_{50}}$ ([0.0025 m, 0.3 m], 11 steps). Model performance was assessed using four different metrics (see below). All metrics are based upon the difference between modeled (Q_{sm}^0) and measured (Q_{sd}^0) sediment discharge at the glacier terminus; some of the quantities are averaged (indicated by a hat, e.g., $\widehat{Q_w^0}$) over various time aggregations (denoted by subscript k) to gain insights into the model's ability of resolving processes over different time scales (see Section 4.3.1). The four metrics are:

1. The Nash-Sutcliffe efficiency (NSE, (Nash & Sutcliffe, 1970)), which quantifies the model's ability to capture the temporal variability of the data

$$NSE_k = 1 - \frac{\sum(\widehat{Q_{sm}^0} - \widehat{Q_{sd}^0})^2}{\sum(\widehat{Q_{sd}^0} - \overline{Q_{sd}^0})^2}\,, \tag{21}$$

   where $\overline{Q_{sd}^0}$ is mean measured sediment discharge at the glacier terminus over the study period.
2. The Spearman rank correlation ($RANK$) between the time series of measured (Q_{sd}^0) and modeled (Q_{sm}^0) sediment discharge, aggregated here over one season. This quantity is used to quantify the model's ability to capture the long-term interannual variability.
3. The absolute deviation (ERR) between modeled and measured sediment discharge

$$ERR_k = \sum\left(\left|\widehat{Q_{sm}^0} - \widehat{Q^0{}_{sd}}\right|\right). \tag{22}$$

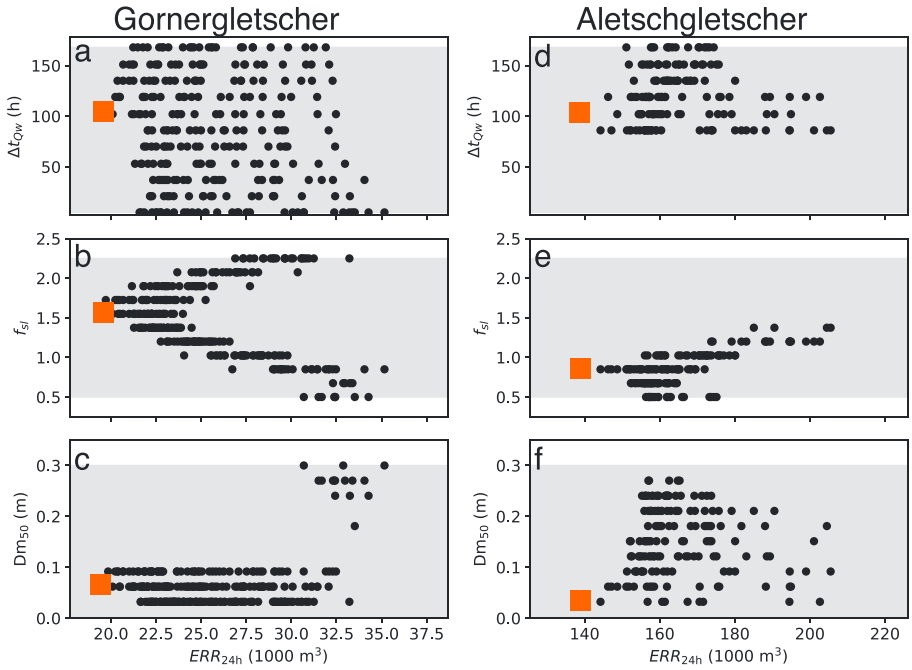

Figure 9. Distribution of the three calibration parameters ($\Delta t, f_{sl}$, and $D_{m_{50}}$) against absolute deviation between modeled and measured sediment discharge (ERR_{24hr}). Only model runs achieving $NSE_{24hr} > 0.5$ are shown. Results are given for Gornergletscher (a–c) and Aletschgletscher (d–f) over the 2016 and 2017 seasons. Parameters used for model runs presented in section 4.3.1 are indicated by orange boxes and listed in Table 6. Gray areas represent the parameter space.

4. The difference (*TERR*) between the total modeled and measured sediment discharge over the entire study period

$$TERR = \left| \sum Q^0_{sm} - \sum Q^0_{sd} \right| . \tag{23}$$

Every model run in the grid search was preceded by a spin-up phase with the corresponding parameter combination. An initial till layer height of $H = 0.75$ m was prescribed, and the model was repeatedly forced with the same hydrological input (taken from the 2 years prior to the actual model start time; see Table 6) until 200 years of simulation had passed or until the mean change in H was less than 0.75 mm/a. This erosion quantity is roughly three-quarters of the measured erosion rates in the region (e.g., Hallet et al., 1996; Stutenbecker et al., 2017). The optimum parameter combination was defined as the one yielding the lowest ERR_{24hr}, with the additional constraint that $NSE_{24hr} > 0.5$ (in experiments comparing seasonal data) or $RANK > 0.8$ for Griesgletscher and $RANK > 0.5$ for Gornergletscher for experiments comparing annual data.

To put the model performance into context, the results were compared to the empirical relationship between sediment and water discharge proposed by Delaney, Bauder, Werder, et al. (2018). The relation is of the form

$$\widehat{Q^0_s} = (a + bt)\left(\widehat{Q^0_w}\right)^c \widehat{Q^0_w}\ \rho_s^{-1}, \tag{24}$$

where a, b, and c are empirical coefficients determined by minimizing ERR_k (equation (22)) and t is time since 10 May of the considered year. The term $(a + bt)\left(\widehat{Q^0_w}\right)^c$ captures sediment concentration, where a and b describe how sediment connectivity evolves through the season, and c describes the sensitivity of the till mobilization to water discharge Delaney, Bauder, Werder, et al. (2018). Values of c both above and below 1 have been found by Delaney, Bauder, Werder, et al. (2018), suggesting that Q_w can have either an amplified or muted effect on sediment discharge.

4.3. Results

4.3.1. Performance of Model's Sediment Discharge on Subannual Timescales

Comparison of model outputs with the data from Gornergletscher and Aletschgletscher over the 2016 and 2017 seasons allows assessment of the model's performance on subannual timescales. Examination of model

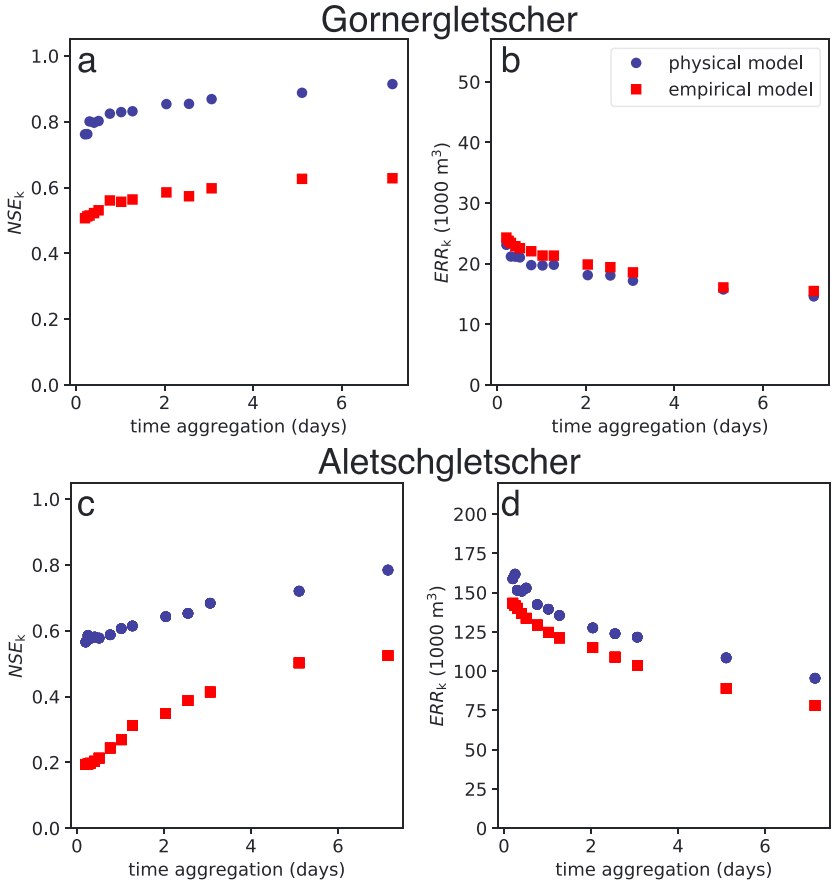

Figure 10. (b, d) Absolute error (ERR_k) and (a, c) Nash-Sutcliffe efficiency (NSE_k) for the numerical model (blue dots) and the empirical relation (red squares, Delaney, Bauder, Werder, et al., 2018). Note that the model outputs from the grid search were evaluated over each time aggregation and that only the best performing run is shown. The parameter combinations may thus vary between time aggregations.

errors at the 24-hr time aggregation from the grid search permits the model sensitivity to the tuning parameters to be constrained. The tuning parameters vary substantially among glaciers (Figure 9 and Table 6) and may indicate different processes controlling sediment discharge from Gornergletscher and Aletschgletscher. For both glaciers, the model performance is highly dependent on f_{sl} and $D_{m_{50}}$. The range of f_{sl} values, which control the glacier's bedrock erosion rate (equations (16) and (17)), is far narrower at Aletschgletscher and has a more pronounced effect there than at Gornergletscher. Conversely, values of $D_{m_{50}}$ for Gornergletscher span a far narrower range and are smaller than for Aletschgletscher. At Aletschgletscher, high values of Δt are required to yield adequate skill (Figure 9), suggesting that high water velocities might be needed at this glacier to transport sediment. At Gornergletscher, by contrast, processes captured by the till model, including sediment connectivity and bedrock erosion, are of primary importance compared to the water's sediment transport capacity, largely controlled by Δt. Similar to subglacial sediment dynamics (Delaney, Bauder, Werder, et al., 2018), the relative importance of tuning parameters can vary substantially from glacier to glacier (Table 6 and Figure 9, orange squares). High variability can particularly be noted for f_{sl}, suggesting that differences in bedrock erosion are a primary factor for the variability in subglacial sediments transport.

The model outputs from the grid search were evaluated at aggregation time periods ranging from approximately 5 hr to 7 days (Figure 10). Performance metrics generally improve when aggregating the results over longer intervals (Figure 10), although the rate of improvement diminishes for aggregations longer than approximately 1 day. This suggests that while the model can capture diurnal variations with reasonable skill (section 3.4), it is better suited to capturing variations in sediment and water discharge at the diurnal time scale and longer, while it has less ability in representing subdaily evolution. This is not particularly surprising

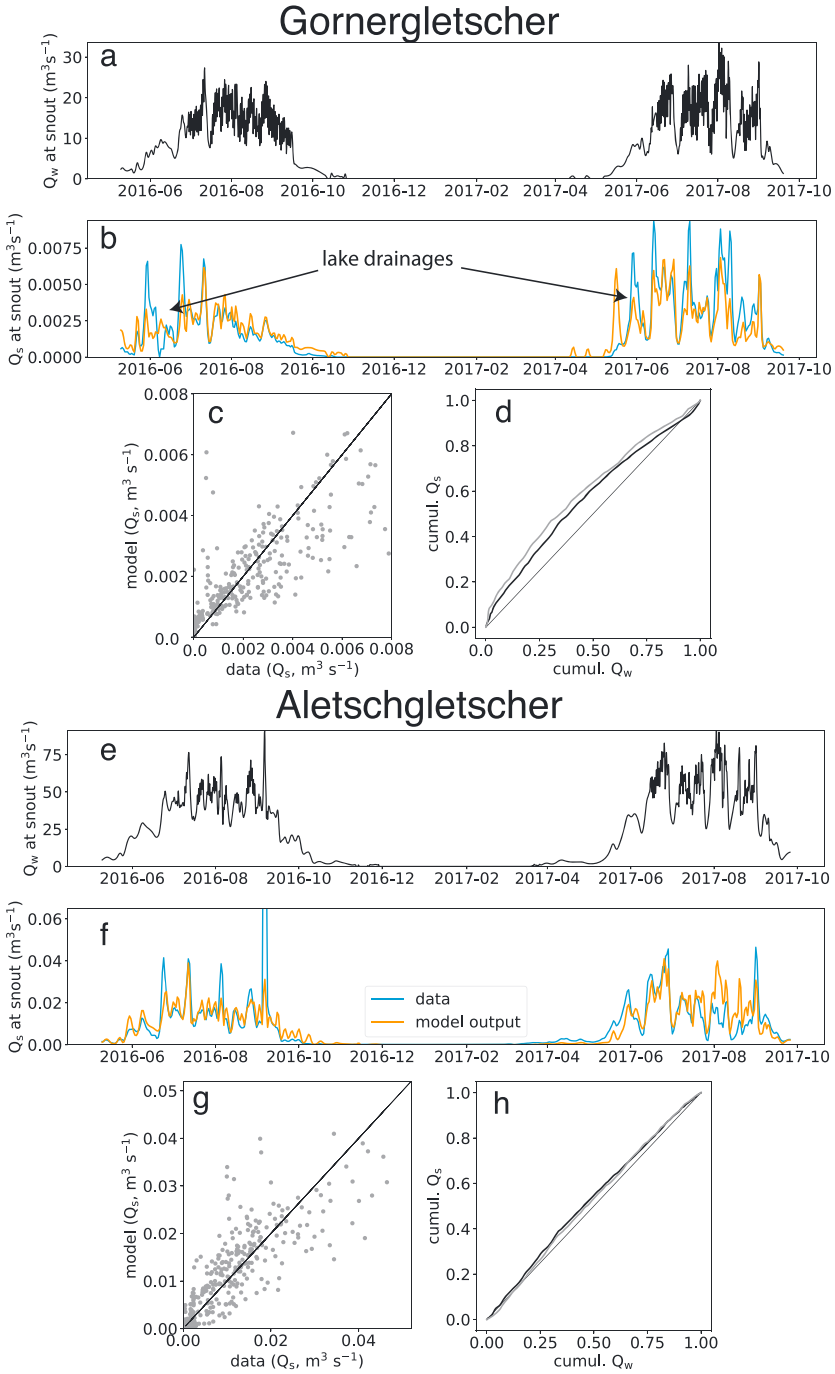

Figure 11. (a, e) Measured water discharge (Q_w) and (b, f) measured and modeled sediment discharge (Q_s^0) over the 2016 and 2017 seasons. Sediment discharge is averaged over 12 hr for both glaciers. Scatter plots (c, g) show measured and modeled sediment discharge averaged over the same period. (d, h) Normalized cumulative amounts of modeled sediment discharge and water discharge over 2016 (black) and 2017 (gray).

since the model neglects englacial storage, and implicitly assumes an instantaneous link between subglacial drainage and changes in sediment discharge at the glacier terminus (section 4.1.4).

Both points are in contrast to the observation that water and sediment can take up to several hours to pass through the subglacial drainage system (Figure 8; Werder and Funk (2009) and Delaney, Bauder, Werder, et al. (2018)).

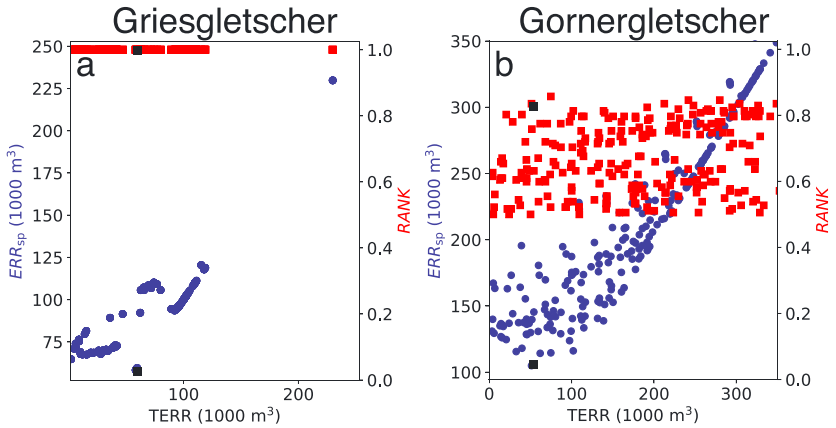

Figure 12. Total error (TERR) compared to absolute error (ERR_{sp}, blue dots, left axis) and rank correlation (*RANK*, red squares, right axis) for the annual time series at Griesgletscher (a) and Gornergletscher (b). Selected model runs are denoted by black squares.

Compared to the empirical relation by Delaney, Bauder, Werder, et al. (2018), the numerical model presented here shows higher NSE_k values (Figure 10). This indicates the improved capacity of the numerical model to reproduce the observed sediment discharge variability (e.g., Delaney, Bauder, Werder, et al., 2018; Swift et al., 2005). The improved reproduction of this variability is due to the incorporation of more sophisticated processes of sediment dynamics in the numerical model, such as till storage, which are needed to capture peak sediment discharge events. The absolute deviation between modeled and measured sediment discharge (ERR_k), instead, is similar to the empirical relation.

Figure 11 shows model outputs with the parameter combinations that yield the smallest ERR_{24hr} over the 2016 and 2017 seasons (Gornergletscher: $ERR_{24hr} = 19,700\,\mathrm{m}^3$, Aletschgletscher: $ERR_{24hr} = 139,400\,\mathrm{m}^3$; Figure 9). The corresponding NSE_{24hr} was 0.83 and 0.56 for Gornergletscher and Aletschgletscher, respectively. Seasonal variations in sediment discharge are captured reasonably well, and performance of the model is consistent across the season (Figures 11b, 11d, 11f, and 11h). The relations between cumulative water discharge and cumulative modeled sediment discharge (Figures 11d and 11h) show strong concave-down shapes. A similar shape occurs in the measurements from these glaciers as well and suggests decreasing till availability through the melt season (Delaney, Bauder, Werder, et al., 2018). Even in 2016, when sediment discharge at Gornergletscher diminished at the end of the season (Figures 11b and 11d), the model can account for the seasonal variations in till availability (Delaney, Bauder, Werder, et al., 2018). The drainages of the ice marginal lake are poorly captured by the model, however, due to both the low water discharge during those events and the model's parameterization of sediment availability (section 5). Aside from these drainage events at Gornergletscher and the peak event at Aletschgletscher in 2016, the model successfully captures numerous smaller sediment discharge events through the season. This highlights the model's capabilities but also points to limitations in its capture of extreme events. It has been suggested that these may activate a more extensive drainage system (e.g., Werder & Funk, 2009), thus increasing the access of meltwater to till. This process is not represented in the model.

4.3.2. Ability of the Model to Capture Interannual Variability

To assess the model's ability to capture interannual variations, multiyear data sets from Gornergletscher (13 years) and Griesgletscher (5 yr and 4 data points) were utilized (section 4.1). Model outputs were aggregated from their original resolution (~5 hr) to the length of the sampling periods (denoted by subscript sp; sections 4.1.1, 4.1.3), and *RANK* and *ERR* were calculated for each period.

Over the study periods, the best model runs yielded $ERR_{sp} = 58,300\,\mathrm{m}^3$ for Griesgletscher ($TERR = 2,038\,\mathrm{m}^3$ or 1.5 % of the total measured sediment discharge, $RANK = 1$) and $ERR_{sp} = 105,000\,\mathrm{m}^3$ for Gornergletscher ($TERR = 3,000\,\mathrm{m}^3$ or 0.7 % of the total measured sediment discharge, $RANK = 0.85$). Note that for Griesgletscher model runs with lower *TERR* are possible but come at the expense of poorer ERR_{sp} (Figure 12). These metrics indicate that the model is mostly capable of accurately capturing interannual variability and total sediment amounts over multiyear periods. Over the decade-long simulation at Gornergletscher, *RANK* remains as high as 0.86, even if *ERR* performs poorly (Figure 12, red dots). This shows

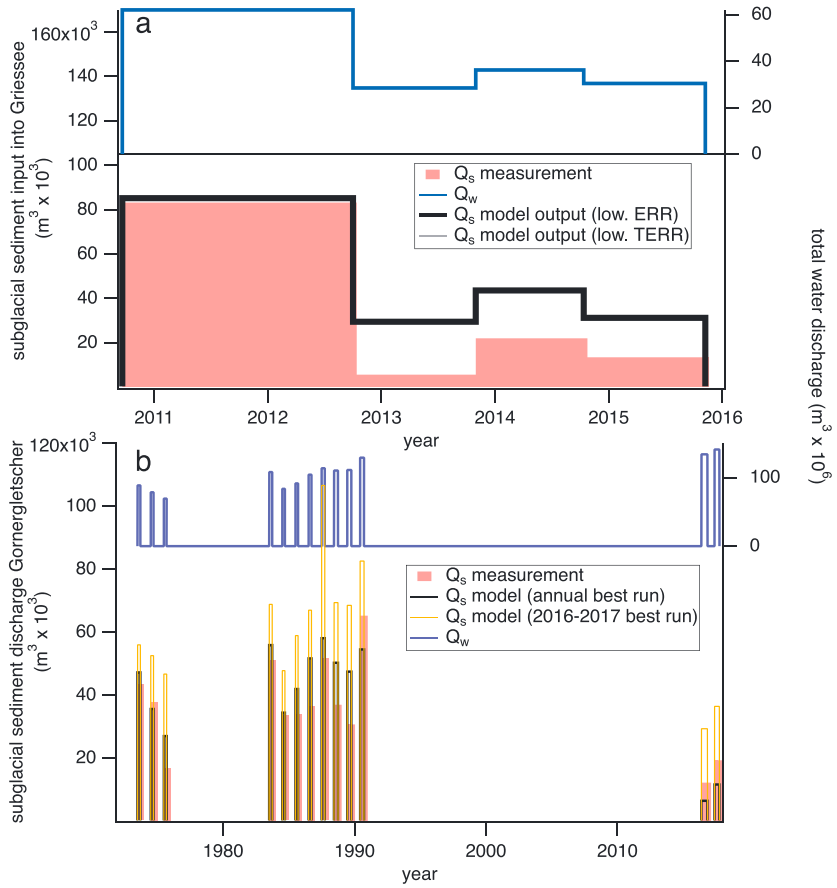

Figure 13. Measured sediment discharge (red), water discharge (blue), and modeled sediment discharge for Griesgletscher (a) and Gornergletscher (b) for the best run over the entire study period (black) and using the 2016–2017 calibration parameters for Gornergletscher (orange).

that interannual variability can mainly be captured, although the exact amounts of sediment discharge are affected by considerable uncertainty.

Note that the glacier topography used during the simulations was held constant, which is in contrast to the large glacier retreat observed at Gornergletscher over the study period. This certainly has caused substantial changes in glacier shape and in the subglacial drainage system (e.g., Fischer et al., 2005) and thus in the amounts of transported sediments (Walder & Fowler, 1994). These unaccounted changes could partially explain the reduced model performance over the decade-long simulation. Additionally, as discussed in Delaney, Bauder, Werder, et al. (2018), the low sediment discharge in 2016 and 2017 could be the result of different instrumentation employed between the two periods.

At Griesgletscher, the anomalously high sediment discharge in 2011–2012 is captured by the model. The overall skill of the model, however, is lessened by the overestimation of sediment discharge in subsequent years. Other model runs with different parameter combinations are better at capturing the variations in sediment discharge from these subsequent years but at the expenses of the peak in 2011–2012. This suggests that the high sediment discharge during this year might have resulted, in part, from changes to till availability, which is difficult for the one-dimensional model to capture (section 5.2).

To further test the model's applicability to decadal time scales, the parameter set determined for Gornergletscher by calibrating the model over 2016–2017 (section 4.3.1) was used to model Gornergletscher's sediment discharge over 1973–2017 (Table 6 and Figure 13). The ERR_{sp} and *RANK* values of this model run were 321, 000 m^3 and 0.80, respectively, indicating that the ability of the model to capture interannual variability with that parameter set is limited. It must be noted, however, that *RANK* improves substantially (*RANK* = 0.67) when the last 2 years of the simulations (2016 and 2017) are excluded.

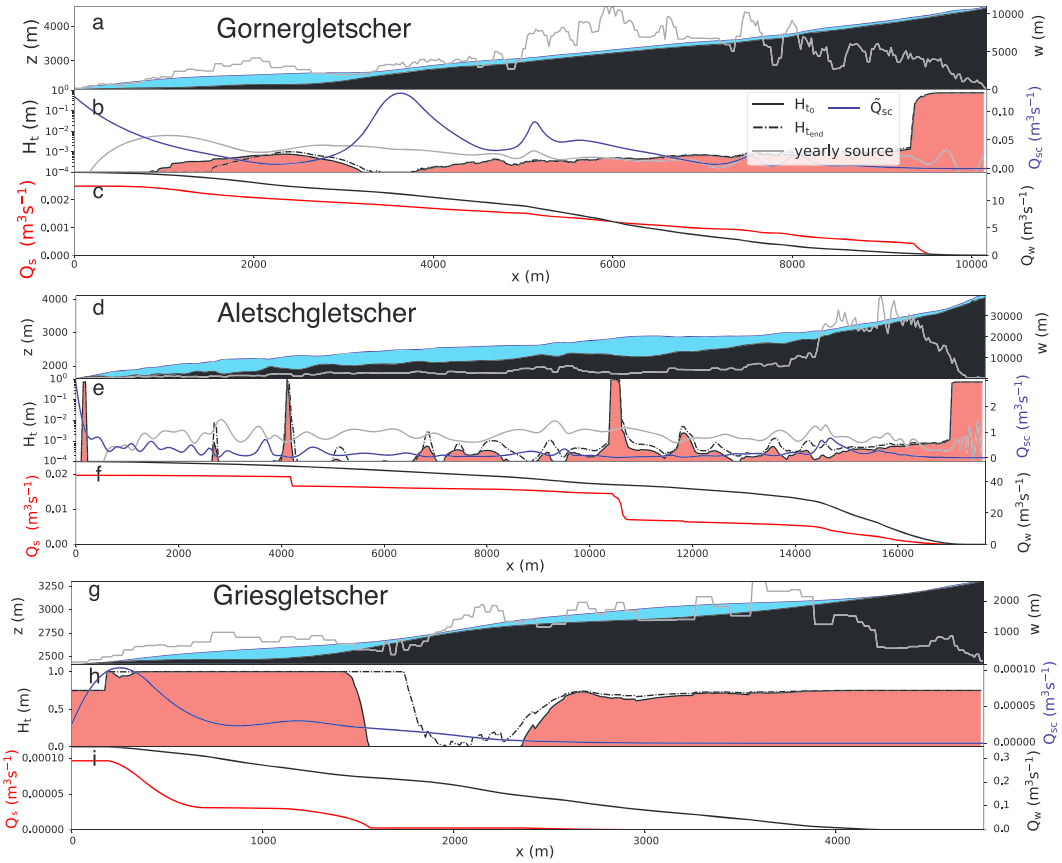

Figure 14. Longitudinal profiles from the three test cases presented in Table 6 (case for Gornergletscher over prolonged time spans omitted). (a, d, g) Glacier geometry showing the elevation of glacier bed (black), ice (blue), and glacier width (gray line). (b, e, h) Sediment discharge capacity ($\tilde{Q}_{sc}$) and till layer height at the beginning (H_0) and at the end (H_t) of the model simulations, together with the annual sediment input by bedrock erosion (gray line; this is very small for Griesgletscher). Note the logarithmic scale in (b) and (e). (c, f, i) Sediment discharge ($\tilde{Q}_s$) and water discharge ($\tilde{Q}_w$) averaged over July and August of the last modeled year.

The above are important improvements when compared to the results of the empirical model ($ERR_{sp} = 235,000\,m^3$, $RANK = 0.13$ over the whole period and $RANK = 0.44$ when excluding 2016 and 2017). Again, this indicates that the physical model has skill in capturing some of the observed interannual variability.

4.3.3. Distribution of Till at the Glacier Bed and Mechanisms of Subglacial Sediment Transport

Because the model operates by evolving a subglacial till layer (section 2.2), the distribution of till at the glacier bed can be estimated, in addition to the sediment discharge. This section examines the amount of till present at the end of the highest-performing model run from each glacier (Table 6, lines 1–3, Figure 9).

Model outputs from Gornergletscher and Aletschgletscher show relatively little till at the glacier bed over the study period, although substantial sediment is deposited in overdeepenings at both glaciers (Figures 14b and 14e; Alley et al., 2003; Creyts et al., 2013). Conversely, the calibrated run for Griesgletscher results in large amounts of sediment at the glacier bed. Here, the model outputs suggest that the majority of the sediment transport takes place in the middle of the glacier, where the hydraulic gradient steepens, whereas little sediment is transported on the upper reaches of the glacier. Again, substantial amounts of sediment are deposited within the overdeepening, where the hydraulic gradient is smaller (Figure 14i). The till layer height reaches H_{lim} at this location, causing the sediment to be passed further downstream (equation (10b)). This also causes the model to quickly respond to sediment transport conditions driven by hydrology but leads to an overestimate in sediment availability when compared to the measurements (Figure 13). The very small bedrock erosion rates should be noted. These are due to the shallow and thin nature of the glacier and to the large amount of accumulated till which prevents further till production (equation (15)).

At both Gornergletscher and Aletschgletscher the modeled sediment transport capacity far exceeds sediment transport (Figures 14b and 14c and 14 and 14f). In many places, this leaves only a few millimeters of till over the bed of both glaciers (Figures 14b and 14e). The presence of this till allows the model to resolve the seasonal evolution of sediment discharge, such as the strong concave-down shapes in Figures 11d and 11h. Observed high sediment transport conditions (Figure 11), however, can be captured in part because till remains at the glacier bed in places such as overdeepenings (e.g., Creyts et al., 2013, Figure 14b) and on upper reaches of the glacier bed (Figures 14b and 11e). The persistence of small amounts of sediment at the glacier bed and the model's ability to capture variations in sediment transport are due to the parameterization of sediment connectivity, discussed in section 5.2, as well as sediment immediately available for transport, which are created from bedrock erosion and from overdeepenings.

5. Discussion

5.1. Model Prospectives

The model relies on a one-way coupling between hydraulics (section 2.1) and till dynamics (section 2.2). Since the till dynamics do not affect the subglacial hydraulics in the model, the till height limit H_{lim} must be prescribed to avoid unbounded subglacial till deposition, particularly in overdeepenings (Alley et al., 2003; Creyts et al., 2013). While overdeepenings do reduce the sediment transport capacity of subglacial water (Alley et al., 2003; Creyts et al., 2013), they certainly do not prevent all sediment from being transported through them (Delaney, Bauder, Werder, et al., 2018). This is particularly evident in the Griesgletscher test case, where model outputs suggest that large amounts of sediment are deposited in the lower part of the glacier (Figure 14h). In other subglacial sediment transport frameworks (Creyts et al., 2013; Walder & Fowler, 1994), deposition of subglacial sediment results in the closure of subglacial conduits and hence in an increase of the hydraulic gradient and water velocities, which increases sediment transport. Some studies have suggested that thick till layers lie below glaciers (e.g., Cook & Swift, 2012; Truffer et al., 1999). The model presented here probably represents the actual till height in these places poorly; however, the model can be used to identify regions of a glacier's bed where substantial amounts of till can persist. The model's simplicity also means that many physical processes thought to occur at the base of a glacier have had to be parameterized, including the armoring of the bed against erosion (through H_g; equation (15)) and the effect of nonchannelized drainage (via $D_{\text{h mi}}$).

The seasonal transition from a distributed drainage system to a channelized drainage system (Iken & Bindschadler, 1986) affects the evacuation of subglacial sediment (Swift et al., 2005). However, this evolution in drainage efficiency is not captured in the hydraulics model, as the hydraulic connectivity, expressed by s in equation (1), is fixed. Such constraints are common to subglacial hydraulics models, and their effects can be minimized by evolving the hydraulic connectivity over the melt season (Downs et al., 2018). In this model, the fixed drainage efficiency likely leads to underestimates of sediment availability and overestimates of sediment transport capacity by increased water velocity early in the season. Such processes could be accounted for by evolving the Hooke angle β (equation (2)) or sediment connectivity factor $\Delta\sigma$ over a season, but such a scheme also adds to the model's complexity.

Our model uses a linear relationship between bedrock erosion and basal sliding, although Koppes et al. (2015) and Herman et al. (2015) suggested that nonlinear relationships better capture bedrock erosion by abrasion. Bedrock erosion is included in this model since the sediment must be supplied to the glacier bed in order for it to be fluvially transported; thus, this somewhat crude scheme is implemented. Attempts to implement these nonlinear relationships (e.g., Herman et al., 2015; Koppes et al., 2015) yielded subglacial till production rates that were too small, unless unrealistic values of f_{sl} were used. We attribute this discrepancy to our parameterization of sliding speed, which is presumed to be related to ice deformation (equation (17); e.g., Huss & Farinotti, 2014), although there are reasons why this assumption is misleading (Beaud et al., 2014; Herman et al., 2011) and in the case of ice streams, even wrong (Cuffey & Paterson, 2010). The discrepancy points to poor constraints on erosional processes, such as glacier plucking (e.g., Alley et al., 1997) or glacier abrasion (e.g., Beaud et al., 2014; Herman et al., 2011, 2015; Koppes et al., 2015), as well as the sliding velocities of the glacier (e.g., Iken & Bindschadler, 1986). Because erosion is treated as a source term in this framework (equation (9)), more sophisticated erosion schemes can, and should, be implemented in future applications of the model. This could include implementation of a coupling between hydrology and bedrock erosion (e.g., Beaud et al., 2014; Herman et al., 2011; Ugelvig et al., 2018).

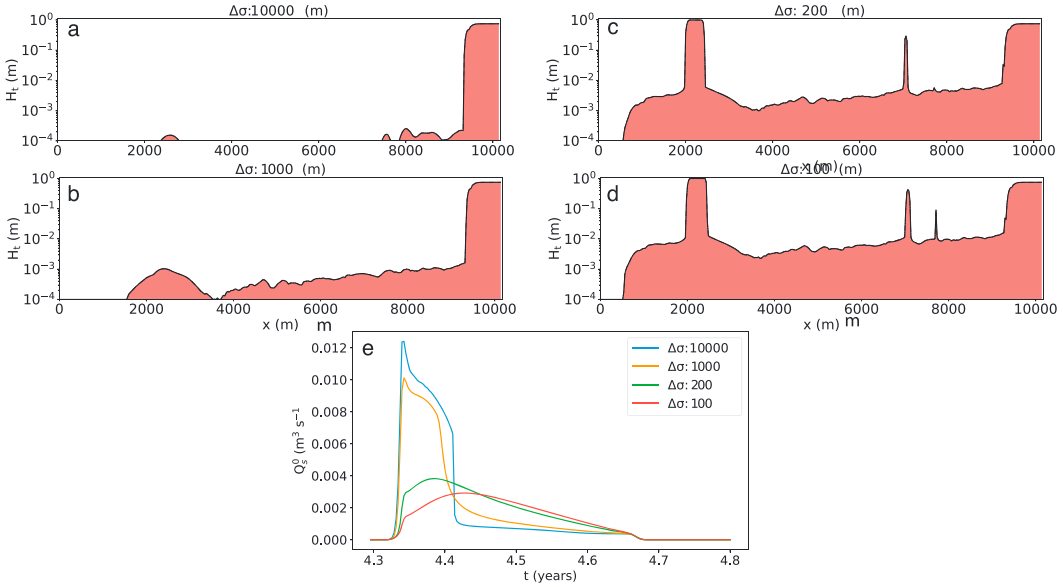

Figure 15. Model response to sediment connectivity for Gornergletscher (a–d) and the synthetic test case (e). Panels (a)–(d) represent till heights H along the bed of Gornergletscher at the completion of the model runs for different sediment connectivity factors $\Delta\sigma$. Panel (e) shows time series of Q_s^0 for the synthetic test case $\Delta T = 4\,^{\circ}\mathrm{C}$; $A_d = 1\,^{\circ}\mathrm{C}$ with different values of $\Delta\sigma$.

The examination of the calibrated tuning parameters Δt, f_{sl}, and $D_{m_{50}}$ also shows that, in some cases, unrealistic values are required to attain reasonable agreement between the modeled and observed sediment quantities (Figure 9). Calibrated values for $D_{m_{50}}$, for instance, do not fall in a typical range for suspended sediments. This is because the model fails to account for processes such as shielding of subglacial sediment or preferential transport of smaller sediments (Dietrich et al., 1989). The corresponding effects are partially offset by the elevated values of $D_{m_{50}}$. Other modeling studies examining subglacial sediment processes have required large sediment size to produce reasonable results (Beaud et al., 2016, 2018). Thus, though the large values of $D_{m_{50}}$ are unreasonable, they are not necessarily cause for alarm.

5.2. Sediment Connectivity

The results of this numerical model suggest that transport capacity is often far in excess of actual sediment discharge (e.g., Figure 14). This means that sediment availability to the meltwater must limit the actual transport. Indeed, field observations suggest that subglacial sediment connectivity varies from glacier to glacier and that variations in sediment discharge occur in response to water discharge even when only limited amounts of sediment persist at the glacier bed (Delaney, Bauder, Werder, et al., 2018; Swift et al., 2005; Willis et al., 1996). The access of subglacial water to sediment is therefore an important process limiting sediment discharge. This factor limits sediment discharge at the beginning of the season (when till produced over winter is potentially available) and increases it at the end, and similar processes have been extensively explored in fluvial environments (e.g., Bracken et al., 2015).

In our one-dimensional model, lateral sediment connectivity is controlled by the sediment connectivity factor $\Delta\sigma$, which decreases sediment mobilization when the till layer drops below a critical thickness (equation 10c). The parameter is empirical, yet it captures observed physical processes, where elevated sediment discharge allows for additional sediment sources to be activated even when relatively small amounts of sediment are available (Figure 3; e.g., Swift et al., 2005; Delaney, Bauder, Werder, et al., 2018). Again, similar processes have been described for fluvial environments where peak discharge events contribute far more to sediment transport compared to more steady discharge cycles (Kirchner et al., 2001; Wolman & Miller, 1960).

To assess the impact of the sediment connectivity factor $\Delta\sigma$, we reran the model for one synthetic test case (Figure 15 e) and examined the results for Gornergletscher with different $\Delta\sigma$ values (Table 7 and Figures 15a–15d).

Table 7
Sensitivity of Model Skill With Respect to $\Delta\sigma$

$\Delta\sigma$ (m^{-1})	NSE_{24hr} ( )	ERR_{24hr} (m^3)
10,000	0.63	29,200
1000	0.81	20,400
200	0.73	23,200
100	0.70	24,100

Note. The best performance from Gornergletscher grid search at 24-hr time aggregation for the high-resolution runs.

Results from the synthetic test case indicated that larger $\Delta\sigma$ (corresponding to increased sediment connectivity) results in a situation where all sediments are evacuated at the beginning of the season, shortly after the onset of meltwater input (Figure 15e). Following the initial pulse, sediment discharge remains at the erosion rate until the end of the season, regardless of meltwater input. In the cases with lower values of $\Delta\sigma$, sediment discharge is maintained throughout the melt season and varies with hydrology as noted in field observations (e.g., Swift et al., 2005; Willis et al., 1996).

For Gornergletscher, values of $\Delta\sigma = 1,000\,m^{-1}$ result in the best model performance. This value of $\Delta\sigma^{-1}$ is on the order of the erosion rates in the catchment (1 mm/a; e.g., Delaney, Bauder, Werder, et al., 2018; Stutenbecker et al., 2017), although further investigation would be necessary to determine whether this is a coincidence or whether a true correspondence exists between $\Delta\sigma$ and erosion rate. Lower values of $\Delta\sigma$ result in lower model skill because till is not exhausted and the seasonal evolution of sediment discharge is captured less well (Figure 15). The experiments for both the synthetic and the real-world case suggest that considering sediment connectivity is necessary when modeling subglacial sediment transport.

6. Conclusions and Future Implications

A numerical model for subglacial sediment transport couples a hydraulics model based on the Darcy-Weisbach-Röthlisberger formulation with a sediment transport model and a till dynamics model that account for till height evolution and production through glacial erosion. The model allows one to assess the access of meltwater to till, the distribution of till along the glacier bed, and the sediment discharge from the glacier snout.

Synthetic test cases show that once an equilibrium is reached between sediment discharge and bedrock erosion, changes in meltwater input affect the timing of the seasonal peak in sediment discharge. The changes in meltwater input have, however, only a marginal influence on the total quantity of sediment evacuated over a season (Figures 5 and 6 and Table 5). Application of the model to three different sites in the Swiss Alps illustrates its ability to reproduce real-world observations—in particular, to capture the total amounts of discharged sediments and the events of peak sediment discharge. Model performance is found to be sensitive to the time interval over which the results are aggregated, the best results being achieved for time aggregations longer than approximately 1 day (Figure 10). We suggest that the weaker performance for subdaily aggregations is caused by the model's instantaneous transport of sediment and negation of englacial water storage. Interannual variability and total sediment quantities are reasonably well captured over periods of up to 44 years (Figure 13 and 12).

A conceptual shortcoming of the model is that the till dynamics model does not feedback to the glacier's hydraulics and dynamics. Yet, the model's performance in real-world cases indicates that neglecting this coupling does not preclude it from adequately describing subglacial sediment discharge. Including feedbacks between hydraulics and subglacial sediment discharge would not only allow for some ad-hoc conditions to be removed (such as limiting the till height in equation (10b)) but could also provide further insight into the interactions between sediment and glaciers. These include the formation of eskers (e.g., Beaud et al., 2018; Hewitt & Creyts, 2019), subglacial hydrology (e.g., Walder & Fowler, 1994), diurnal glacier uplift (Perolo et al., 2018), the effect of till on glacier sliding (e.g., Truffer et al., 2001), processes in glacial overdeepenings (e.g., Cook & Swift, 2012; Creyts et al., 2013), and creation of sediment shoals in tidewater glaciers (e.g., Brinkerhoff et al., 2017).

The model outputs based upon inputs and calibration to the Swiss glaciers suggest that variations in subglacial sediment discharge over time periods of up to one season are mostly a result of changes in sediment transport capacity, thus showing the control exerted by the hydrological input, as opposed to bedrock erosion. The access of meltwater to till controls the response of sediment transport to hydrology, which is represented through the sediment connectivity factor $\Delta\sigma$ (Figure 15). By contrast, over longer time periods, bedrock erosion is of primary importance for sediment discharge (Hallet, 1979; Iverson, 2012). In the model, this is captured by the strong dependence of till production on the sliding fraction f_{sl} (Figure 9). The Gorner, Gries, and Aletsch glaciers examined here show relatively moderate hydraulic gradients, although subglacial erosion on steep glaciers with steep gradients has been shown to be highly variable even on subseasonal timescales (Herman et al., 2015). Better constraints on short-term variations of bedrock erosion (e.g., Beaud et al., 2014; Herman et al., 2015; Ugelvig et al., 2018) would be helpful for future model applications, as this information could be used to separate sediment discharge that is driven by sediment transport conditions from sediment discharge that is driven by changes in sediment connectivity.

The relatively simple framework presented here is more effective in capturing quantities and trends in subglacial sediment discharge than empirical relations presented previously (Delaney, Bauder, Werder, et al., 2018). Most processes included in the presented model have an established theoretical underpinning, such as R-channel drainage (Röthlisberger, 1972), subglacial erosion (e.g., Hallet, 1981) and sediment transport (Creyts et al., 2013; Walder & Fowler, 1994). Refining the glacier erosion scheme, or including processes of englacial water storage, however, could provide the means to further increase the model's capabilities. Future work should also focus on describing processes that regulate the connectivity between subglacial water and stored till, as this has only received little attention in the literature (Collins, 1996; Swift et al., 2005; Willis et al., 1996). Extending the model to two dimensions, or considering both efficient and inefficient drainage systems, could serve to better constrain sediment connectivity processes.

We anticipate that the model framework can prove a useful tool for stakeholders, engineers, and scientists who wish to understand how sediment dynamics in alpine regions responds to glacier retreat.

Acknowledgments
This work was funded by the Swiss National Science Foundation (SNSF) National Research Programme (NRP) 70 "Energy Turnaround", Project 153927. M. Funk, D. Vetsch, and A. Siviglia provided many insightful comments and useful suggestions. We thank the three reviewers, R. LeB. Hooke, D. Swift, and M. Truffer for their thoughtful and insightful comments which have greatly improved this manuscript. Sediment discharge data used to tune the model are available online (10.3929/ethz-b-000333310). Julia (julialang.org) scripts used to run the real-world and synthetic applications are available online (bitbucket.org/IanDelaney/jgr_2019). Glacier topography and terminus melt data can be found online (10.3929/ethz-b-000352105). Finally, the model itself, SUGSET.jl, can be found online (bitbucket.org/IanDelaney/sugset.jl). We encourage readers with interests in subglacial sediment dynamics to explore and critique its capabilities and applications.

References

Alley, R. B., Cuffey, K. M., Evenson, E. B., Strasser, J. C., Lawson, D. E., & Larson, G. J. (1997). How glaciers entrain and transport basal sediment: Physical constraints. *Quaternary Science Reviews*, *16*(9), 1017–1038.

Alley, R. B., Lawson, D. E., Larson, G. J., Evenson, E. B., & Baker, G. S. (2003). Stabilizing feedbacks in glacier-bed erosion. *Nature*, *424*(6950), 758–760.

Anselmetti, F. S., Bühler, R., Finger, D., Girardclos, S., Lancini, A., Rellstab, C., & Sturm, M. (2007). Effects of Alpine hydropower dams on particle transport and lacustrine sedimentation. *Aquatic Sciences*, *69*(2), 179–198.

Ballantyne, C. K. (2002). A general model of paraglacial landscape response. *The Holocene*, *12*(3), 371–376.

Beaud, F., Flowers, G. E., & Pimentel, S. (2014). Seasonal-scale abrasion and quarrying patterns from a two-dimensional ice-flow model coupled to distributed and channelized subglacial drainage. *Geomorphology*, *219*, 176–191.

Beaud, F., Flowers, G. E., & Venditti, J. G. (2016). Efficacy of bedrock erosion by subglacial water flow. *Earth Surface Dynamics*, *4*(1), 125–145. https://doi.org/10.5194/esurf-4-125-2016

Beaud, F., Flowers, G. E., & Venditti, J. G. (2018). Modeling sediment transport in ice-walled subglacial channels and its implications for esker formation and pro-glacial sediment yields. *Journal of Geophysical Research: Earth Surface*, *123*, 3206–3227. https://doi.org/10.1029/2018JF004779

Bendixen, M., Iversen, L. L., Bjørk, A. A., Elberling, B., Westergaard-Nielsen, A., Overeem, I., et al. (2017). Delta progradation in Greenland driven by increasing glacial mass loss. *Nature*, *550*(7674), 101.

Bezinge, A. (1987). Glacial meltwater streams, hydrology and sediment transport: The case of the Grande Dixence hydroelectricity scheme. In A. M. Gurnell, & M. J. Clark (Eds.), *Glacio-fluvial sediment transfer: An Alpine perspective* (pp. 473–498). Chichester: John Wiley.

Bracken, L. J., Turnbull, L., Wainwright, J., & Bogaart, P. (2015). Sediment connectivity: A framework for understanding sediment transfer at multiple scales. *Earth Surface Processes and Landforms*, *40*(2), 177–188.

Brinkerhoff, D., Truffer, M., & Aschwanden, A (2017). Sediment transport drives tidewater glacier periodicity. *Nature Communications*, *8*(90), 90.

Brown, L. E., Hannah, D. M., & Milner, A. M. (2007). Vulnerability of alpine stream biodiversity to shrinking glaciers and snowpacks. *Global Change Biology*, *13*(5), 958–966.

Burke, M. J., Brennand, T. A, & Sjogren, D. B. (2015). The role of sediment supply in esker formation and ice tunnel evolution. *Quaternary Science Reviews*, *115*, 50–77.

Carter, S. P., Fricker, H. A., & Siegfried, M. R. (2017). Antarctic subglacial lakes drain through sediment-floored canals: Theory and model testing on real and idealized domains. *The Cryosphere*, *11*, 381–405.

Chen, Y., Liu, X., Gulley, J. D., & Mankoff, KD. (2018). Subglacial conduit roughness: Insights from computational fluid dynamics models. *Geophysical Research Letters*, *45*, 11,206–11,218. https://doi.org/10.1029/2018GL079590

Church, M., & Ryder, J. M. (1972). Paraglacial sedimentation: A consideration of fluvial processes conditioned by glaciation. *Geological Society of America Bulletin*, *83*(10), 3059–3072.

Clarke, G. K. C. (2003). Hydraulics of subglacial outburst floods: New insights from the Spring–Hutter formulation. *Journal of Glaciology*, *49*(165), 299–313.

Collins, D. N. (1979). Sediment concentration in melt waters as an indicator of erosion processes beneath an Alpine glacier. *Journal of Glaciology*, *23*, 247–257.
Collins, D. N. (1989). Seasonal development of subglacial drainage and suspended sediment delivery to melt waters beneath an Alpine glacier. *Annals of Glaciology*, *13*, 45–50.
Collins, D. N. (1990). Seasonal and annual variations of suspended sediment transport in meltwaters draining from an Alpine glacier. In *Proceedings of two lausanne symposia*, *193*, International Association of Hydrological Sciences, pp. 439–446.
Collins, D. N. (1996). A conceptually based model of the interaction between flowing meltwater and subglacial sediment. *Annals of Glaciology*, *22*(1), 224–232.
Cook, S. J., & Swift, D. A. (2012). Subglacial basins: Their origin and importance in glacial systems and landscapes. *Earth-Science Reviews*, *115*(4), 332–372.
Costa, A., Molnar, P., Stutenbecker, L., Bakker, M., Silva, T. A., Schlunegger, F., et al. (2018). Temperature signal in suspended sediment export from an Alpine catchment. *Hydrology and Earth System Sciences*, *22*(1), 509–528.
Creyts, T. T., Clarke, G. K. C., & Church, M. (2013). Evolution of subglacial overdeepenings in response to sediment redistribution and glaciohydraulic supercooling. *Journal of Geophysical Research: Earth Surface*, *118*, 423–446. https://doi.org/10.1002/jgrf.20033
Cuffey, K. M., & Paterson, W. S. B. (2010). *The physics of glaciers* (Forth). Burlington, MA, USA: Butterworth-Heinemann.
de Fleurian, B, Werder, M. A., Beyer, S., Brinkerhoff, D., Delaney, I., Dow, C., et al. (2018). SHMIP, the subglacial hydrology model intercomparison project. *Journal of Glaciology*, *64*, 897–916.
Delaney, I., Bauder, A., Huss, M., & Weidmann, Y. (2018). Proglacial erosion rates and processes in a glacierized catchment in the Swiss Alps. *Earth Surface Processes and Landfroms*, *43*(4), 765–778.
Delaney, I., Bauder, A., Werder, M. A., & Farinotti, D. (2018). Regional and annual variability in subglacial sediment transport by water for two glaciers in the Swiss Alps. *Frontiers in Earth Science*, *43*, 765–778.
Dietrich, W. E., Kirchner, J. W., Ikeda, H., & Iseya, F. (1989). Sediment supply and the development of the coarse surface layer in gravel-bedded rivers. *Nature*, *340*, 215–217. https://doi.org/10.1038/340215a0
Downs, J., Johnson, J., Harper, J., Meierbachtol, T., & Werder, M. A. (2018). Dynamic hydraulic conductivity reconciles mismatch between modeled and observed winter subglacial water pressure. *Journal of Geophyscial Research: Earth Surface*, *123*, 818–836. https://doi.org/10.1002/2017JF004522
Ehrbar, D., Schmocker, L., Doering, M., Cortese, M., Bourban, G., Boes, R. M., & Vetsch, D. F. (2018). Continuous seasonal and large-scale periglacial reservoir sedimentation. *Sustainability*, *10*(9), 3265.
Engelund, F., & Hansen, E. (1967). A monograph on sediment transport in alluvial streams (Technical report): Technical University of Denmark.
Exner, F. M. (1920a). Über die Wechselwirkung zwischen Wasser und Geschiebe in flüssen. *Abhandlungen der Akadamie der Wissenschaften, Wien*, *134*(2a), 165–204.
Exner, F. M. (1920b). Zur Physik der Dünen. *Abhandlungen der Akadamie der Wissenschaften, Wien*, *129*(2a), 929–952.
Farinotti, D., Huss, M., Bauder, A., & Funk, M. (2009). An estimate of the glacier ice volume in the Swiss Alps. *Global and Planetary Change*, *68*(3), 225–231.
Farinotti, D., Usselmann, S., Huss, M., Bauder, A., & Funk, M. (2012). Runoff evolution in the Swiss Alps: Projections for selected high-alpine catchments based on ENSEMBLES scenarios. *Hydrological Processes*, *26*(13), 1909–1924.
Felix, D., Albayrak, I., Abgottspon, A, & Boes, R. M. (2016). Suspended sediment measurements and calculation of the particle load at hpp fieschertal. *IOP Conference Series: Earth and Environmental Science*, *49*(12), 122007.
Fischer, U. H., Braun, A., Bauder, A., & Flowers, G. E. (2005). Changes in geometry and subglacial drainage derived from digital elevation models: Unteraargletscher, Switzerland, 1927–97. *Annals of Glaciology*, *40*(1), 20–24.
Flowers, G. E., & Clarke, G. K. C. (1999). Surface and bed topography of Trapridge Glacier, Yukon Territory, Canada: Digital elevation models and derived hydraulic geometry. *Journal of Glaciology*, *45*(149), 165–174.
Guillon, H., Mugnier, J. L., Buoncristiani, J. F., Carcaillet, J., Godon, C., Prud'homme, C., et al. (2015). Improved discrimination of subglacial and periglacial erosion using ^{10}Be concentration measurements in subglacial and supraglacial sediment load of the Bossons Glacier (Mont Blanc Massif, France). *Earth Surface Processes and Landforms*, *40*(9), 1202–1215.
Hairer, E., Nørsett, S. P., & Wanner, G. (1993). *Solving ordinary differential equations I: Nonstiff problems* (Vol. 1). Berlin, Heidelberg: Springer Science & Business.
Hallet, B. (1979). A theoretical model of glacial abrasion. *Journal of Glaciology*, *23*(89), 39–50.
Hallet, B. (1981). Glacial abrasion and sliding: Their dependence on the debris concentration in basal ice. *Annals of Glaciology*, *2*, 23–28.
Hallet, B., Hunter, L., & Bogen, J. (1996). Rates of erosion and sediment evacuation by glaciers: A review of field data and their implications. *Global and Planetary Change*, *12*(1), 213–235.
Herman, F., Beaud, F., Champagnac, J. D., Lemieux, J. M., & Sternai, P. (2011). Glacial hydrology and erosion patterns: A mechanism for carving glacial valleys. *Earth and Planetary Science Letters*, *310*(3), 498–508.
Herman, F., Beyssac, O., Brughelli, M., Lane, S. N., Leprince, S., Adatte, T., et al. (2015). Erosion by an alpine glacier. *Science*, *350*(6257), 193–195.
Hewitt, I. J., & Creyts, T. T. (2019). A model for the formation of eskers. *Geophysical Research Letters*, *46*, 6673–6680. https://doi.org/10.1029/2019GL082304
Hock, R. (2003). Temperature index melt modelling in mountain areas. *Journal of Hydrology*, *282*(1), 104–115. Mountain Hydrology and Water Resources.
Hooke, R. LeB., Laumann, T., & Kohler, J. (1990). Subglacial water pressures and the shape of subglacial conduits. *Journal of Glaciology*, *36*(122), 67–71.
Huss, M., Bauder, A., Funk, M., & Hock, R. (2008). Determination of the seasonal mass balance of four Alpine glaciers since 1865. *Journal of Geophysical Research*, *113*, F01015. https://doi.org/10.1029/2007JF000803
Huss, M., & Farinotti, D. (2012). Distributed ice thickness and volume of all glaciers around the globe. *Journal of Geophysical Research*, *117*, F04010. https://doi.org/10.1029/2012JF002523
Huss, M., & Farinotti, D. (2014). A high-resolution bedrock map for the Antarctic Peninsula. *The Cryosphere*, *8*(4), 1261–1273.
Huss, M., & Hock, R. (2018). Global-scale hydrological response to future glacier mass loss. *Nature Climate Change*, *8*(2), 135–140.
Huss, M., Jouvet, G., Farinotti, D., & Bauder, A. (2010). Future high-mountain hydrology: A new parameterization of glacier retreat. *Hydrology and Earth System Sciences*, *14*(5), 815–829.
Hutter, K. (1983). *Theoretical glaciology*. Dordrecht, NL: D. Reidel Publishing Co.
Iken, A., & Bindschadler, R. A. (1986). Combined measurements of subglacial water pressure and surface velocity of Findelengletscher, Switzerland: Conclusions about drainage system and sliding mechanism. *Journal of Glaciology*, *32*(110), 101–119.

Iverson, N. R. (2012). A theory of glacial quarrying for landscape evolution models. *Geology*, *40*(8), 679–682.
Iverson, N. R., & Semmens, D. J. (1995). Intrusion of ice into porous media by regelation: A mechanism of sediment entrainment by glaciers. *Journal of Geophysical Research*, *100*, 10,219–10,230.
Kirchner, J. W., Finkel, R. C., Riebe, C. S., Granger, D. E., Clayton, J. L., King, J. G., & Megahan, W. F. (2001). Mountain erosion over 10 yr, 10 k. y. , and 10 m.y. time scales. *Geology*, *29*(7), 591.
Koppes, M. N., Hallet, B., & Anderson, J. (2009). Synchronous acceleration of ice loss and glacial erosion, Glaciar Marinelli, Chilean Tierra del Fuego. *Journal of Glaciology*, *55*(190), 207–220.
Koppes, M., Hallet, B., Rignot, E., Mouginot, J., Wellner, J. S., & Boldt, K. (2015). Observed latitudinal variations in erosion as a function of glacier dynamics. *Nature*, *526*(7571), 100–103.
Koppes, M. N., & Montgomery, D. R. (2009). The relative efficacy of fluvial and glacial erosion over modern to orogenic timescales. *Nature Geoscience*, *2*(9), 644–647.
Lancaster, S. T., Nolin, A. W., Copeland, E. A., & Grant, G. E. (2012). Periglacial debris-flow initiation and susceptibility and glacier recession from imagery, airborne LiDAR, and ground-based mapping. *Geosphere*, *8*(2), 417–430.
Lane, S. N., Bakker, M., Gabbud, C., Micheletti, N., & Saugy, J. (2017). Sediment export, transient landscape response and catchment-scale connectivity following rapid climate warming and alpine glacier recession. *Geomorphology*, *277*, 210–227.
Mao, L., Dell'Agnese, A., Huincache, C., Penna, D., Engel, M., Niedrist, G., & Comiti, F. (2014). Bedload hysteresis in a glacier-fed mountain river. *Earth Surface Processes and Landforms*, *39*(7), 964–976.
Meyer-Peter, E., & Müller, R. (1948). Formulas for bedload transport. In *International Association for Hydro-Environment Engineering and Research*, Hydraulic engineering reports. Stockholm.
Nash, J. E., & Sutcliffe, J. V. (1970). River flow forecasting through conceptual models part I—A discussion of principles. *Journal of Hydrology*, *10*(3), 282–290.
Ng, F. S. L. (2000). Canals under sediment-based ice sheets. *Annals of Glaciology*, *30*(1), 146–152.
Paola, C., & Voller, V. R. (2005). A generalized Exner equation for sediment mass balance. *Journal of Geophysical Research*, *110*, F04014. https://doi.org/10.1029/2004JF000274
Penck, A. (1905). Glacial features in the surface of the Alps. *The Journal of Geology*, *13*(1), 1–19.
Perolo, P., Bakker, M., Gabbud, C., Moradi, G., Rennie, C., & Lane, S. N. (2018). Subglacial sediment production and snout marginal ice uplift during the late ablation season of a temperate valley glacier. *Earth Surface Processes and Landforms*, *44*, 1–68.
Phillips, B. C., & Sutherland, A. J. (1989). Spatial lag effects in bed load sediment transport. *Journal of Hydraulic Research*, *27*(1), 115–133.
Rackauckas, C., & Nie, Q. (2017). Differential equations. jl–A performant and feature-rich ecosystem for solving differential equations in Julia. *Journal of Open Research Software*, *5*(1), 15.
Radhakrishnan, K., & Hindmarsh, A. C. (1993). Description and use of LSODE, the Livermore solver for ordinary differential equations. Reference Publication 1327, NASA.
Richards, G., & Moore, R. D. (2003). Suspended sediment dynamics in a steep, glacier-fed mountain stream, Place Creek, Canada. *Hydrological Processes*, *17*(9), 1733–1753.
Riihimaki, C. A., MacGregor, K. R., Anderson, R. S., Anderson, S. P., & Loso, M. G. (2005). Sediment evacuation and glacial erosion rates at a small alpine glacier. *Journal of Geophysical Research*, *110*, F03003. https://doi.org/10.1029/2004JF000189
Röthlisberger, H. (1972). Water pressure in intra- and subglacial channels. *Journal of Glaciology*, *11*(62), 177–203.
Röthlisberger, H., & Iken, A. (1981). Plucking as an effect of water-pressure variations at the glacier bed. *Annals of Glaciology*, *2*(1), 57–62.
Shreve, R. L. (1972). Movement of water in glaciers. *Journal of Glaciology*, *11*(62), 205–214.
Sigler, W. V., Crivii, S., & Zeyer, J. (2002). Bacterial succession in glacial forefield soils characterized by community structure, activity and opportunistic growth dynamics. *Microbial Ecology*, *44*(4), 306–316.
Singh, P., Haritashya, U. K., Ramasastri, K. S., & Kumar, N. (2005). Diurnal variations in discharge and suspended sediment concentration, including runoff-delaying characteristics, of the Gangotri Glacier in the Garhwal Himalayas. *Hydrological Processes*, *19*(7), 1445–1457.
Stott, T., & Mount, N. (2007). Alpine proglacial suspended sediment dynamics in warm and cool ablation seasons: Implications for global warming. *Journal of Hydrology*, *332*(3), 259–270.
Stutenbecker, L., Delunel, R., Schlunegger, F., Silva, T. A., Segvić, B., Girardclos, S., et al. (2017). Reduced sediment supply in a fast eroding landscape? A multi-proxy sediment budget of the upper Rhône basin, Central Alps. *Sedimentary Geology*, *375*, 105–119.
Swift, D. A., Cook, S. J., Graham, D. J., Midgley, N. G., Fallick, A. E., Storrar, R., et al. (2018). Terminal zone glacial sediment transfer at a temperate overdeepened glacier system. *Quaternary Science Reviews*, *180*, 111–131.
Swift, D. A., Nienow, P. W., & Hoey, T. B. (2005). Basal sediment evacuation by subglacial meltwater: Suspended sediment transport from Haut Glacier d'Arolla, Switzerland. *Earth Surface Processes and Landforms*, *30*(7), 867–883.
Thapa, B., Shrestha, R., Dhakal, P., & Thapa, B. S. (2005). Problems of Nepalese hydropower projects due to suspended sediments. *Aquatic Ecosystem Health & Management*, *8*(3), 251–257.
Truffer, M., Echelmeyer, K. A., & Harrison, W. D. (2001). Implications of till deformation on glacier dynamics. *Journal of Glaciology*, *47*(156), 123–134.
Truffer, M., Motyka, R. J., Harrison, W. D., Echelmeyer, K. A., Fisk, B., & Tulaczyk, S. (1999). Subglacial drilling at Black Rapids Glacier, Alaska, U.S.A.: Drilling method and sample descriptions. *Journal of Glaciology*, *45*(151), 495–505.
Ugelvig, S. V., Egholm, D. L., Anderson, R. S., & Iverson, N. R. (2018). Glacial erosion driven by variations in meltwater drainage. *Journal of Geophysical Research: Earth Surface*, *123*, 28630–2877. https://doi.org/10.1029/2018JF004680
Walder, J. S., & Fowler, A. (1994). Channelized subglacial drainage over a deformable bed. *Journal of Glaciology*, *40*(134), 3–15.
Warburton, J. (1990). An alpine proglacial fluvial sediment budget. *Geografiska Annaler. Series A, Physical Geography*, *72*(3/4), 261–272.
Werder, M. A. (2016). The hydrology of subglacial overdeepenings: A new supercooling threshold formula. *Geophysical Research Letters*, *43*, 2045–2052. https://doi.org/10.1002/2015GL067542
Werder, M. A., Bauder, A., Funk, M., & Keusen, H. R. (2010). Hazard assessment investigations in connection with the formation of a lake on the tongue of Unterer Grindelwaldgletscher, Bernese Alps, Switzerland. *Natural Hazards and Earth System Science*, *10*(2), 227–237.
Werder, M. A., & Funk, M. (2009). Dye tracing a jökulhlaup: II. Testing a jökulhlaup model against flow speeds inferred from measurements. *Journal of Glaciology*, *55*(193), 899–908.
Werder, M. A., Hewitt, I. J., Schoof, C. G., & Flowers, G. E. (2013). Modeling channelized and distributed subglacial drainage in two dimensions. *Journal of Geophysical Research: Earth Surface*, *118*, 2140–2158. https://doi.org/10.1002/jgrf.20146
Werder, M. A., Schuler, T. V., & Funk, M. (2010). Short term variations of tracer transit speed on alpine glaciers. *The Cryosphere*, *4*(3), 381–396.
Williams, G. P. (1989). Sediment concentration versus water discharge during single hydrologic events in rivers. *Journal of Hydrology*, *111*(1), 89–106.

Willis, I. C., Richards, K. S., & Sharp, M. J. (1996). Links between proglacial stream suspended sediment dynamics, glacier hydrology and glacier motion at Midtdalsbreen, Norway. *Hydrological Processes*, *10*(4), 629–648.
Wolman, M. G., & Miller, J. P. (1960). Magnitude and frequency of forces in geomorphic processes. *The Journal of Geology*, *68*(1), 54–74.
Zekollari, H., & Huybrechts, P. (2015). On the climate0-geometry imbalance, response time and volume-area scaling of an alpine glacier: Insights from a 3-D flow model applied to Vadret da Morteratsch, Switzerland. *Annals of Glaciology*, *56*(70), 51–62.